Raffaella Guida

Abstract: Synthetic Aperture Radar (SAR) represents today one of the most powerful instruments in monitoring the growth of urban centers and its relevant management. New upcoming SAR sensors will soon supply high resolution images with a consequent increase in the information content.

This thesis contributes originally to the topic above, ranging from the simulation to the post-processing of high resolution SAR data. In particular, an efficient SAR raw signal simulator for extended scenes is developed for the hybrid stripmap-spotlight configuration. Moreover, a new model-based approach for geometrical and electromagnetic information retrieval from SAR images of urban areas is defined, widely discussed and finally tested on real high resolution SAR images.

High resolution SAR for urban areas monitoring

2005/06

UNIVERSITA' DEGLI STUDI DI NAPOLI FEDERICO II

Scuola di Dottorato in Ingegneria dell'Informazione

High Resolution SAR for Urban Areas Monitoring

Raffaella Guida

Dottorato di Ricerca in Ingegneria Elettronica e delle Telecomunicazioni

TESI DI DOTTORATO

UNIVERSITA' DEGLI STUDI DI NAPOLI FEDERICO II

DIPARTIMENTO DI INGEGNERIA ELETTRONICA
E DELLE TELECOMUNICAZIONI

DOTTORATO DI RICERCA IN
INGEGNERIA ELETTRONICA E DELLE TELECOMUNICAZIONI

High Resolution SAR for Urban Areas Monitoring

RAFFAELLA GUIDA

Il Coordinatore del Corso
Ch.mo Prof. Giovanni Poggi

Il Tutore
Ch.mo Prof. Giorgio Franceschetti

Anno accademico 2005–2006

Index

Introduction

Nowadays, the availability of a technology able to support the monitoring and management of the earth resources is becoming of extreme importance.

Remote sensing represents, in this topic, one of the most significant player for its distinctive features of not invasive technique and wide range of applications. It is, in fact, the science and art of obtaining information about an object, area, or phenomenon through the analysis of data acquired by a device that is not in contact with the object, area, or phenomenon under investigation. The operation of remotely collecting data, that may be further analyzed to obtain the desired information, is carried on by sensors which can be of different kind as the data they sense and collect are of many forms.

In this thesis we refer to *electromagnetic* energy sensors operating from airborne and spaceborne platforms to assist in inventorying, mapping and monitoring earth resources. In particular, we deeply discuss the capabilities of the Synthetic Aperture Radar in its standard and well known working configuration (Chapter 1) as well as its new operational modes able to guarantee high resolution data (Chapter 2).

In these chapters not only the working geometries and SAR performance are presented but also, for every mode, a possible way to simulate the primary signal collected by the sensor called *raw data*. Simulators, in fact, are important tools supporting the design and project of new sensors and are able to conveniently lead the criterions for setting the mission parameters as they take into accounts the applications they are planned for.

This thesis contributes to the topic of SAR raw signal simulation presenting a new, efficient algorithm for the simulation of SAR raw data acquired in the hybrid stripmap-spotlight configuration, see Chapter 2. The algorithm is also implemented and tested through many simulation examples relevant both to canonical and actual scenes.

After having introduced the different techniques to collect data by SAR sensors, we move to discuss the possibility of retrieving information analyzing those data.

This problem is faced for a particular kind of data represented by images of urban areas. In Chapter 3 we mainly analyze the state of art stressing that many efforts have been made for retrieving geometrical information (shape of buildings and relevant dimensions), while the extraction of electromagnetic parameters, i.e. the dielectric constants of the materials present in the scene, is still taking the first steps.

We also highlight that some qualitative information, retrieved by approaches detailed in literature, is still limited and poor for the lack of models able to sufficiently represent the geometry of urban centers and the way the radar signal interacts with them.

In Chapter 4 a geometrical model for isolated buildings placed on rough terrains and a complete scattering model are introduced. But the novelty of the chapter is showing that the electromagnetic model, taking into account the scene and the radar parameters, can be inverted leading, this time, to a quantitative retrieval of some information contained in the scene.

This inversion procedure, called deterministic approach, is widely discussed and tested, in a first moment, on simulated SAR images for the building height retrieval.

The limits of the method are also underlined. In particular, the need of a high a-priori knowledge of the scene represents a requirement not always fulfilled for the application of the method.

For this reason, a sensitiveness analysis is carried on to understand the robustness of the proposed approach when the ground truth is not precisely known.

After this crucial step, the deterministic approach is applied, for the first time in literature, to real SAR images in Chapter 5.

According to the steps described in Chapter 4, the height of a particular building is retrieved by the double reflection contribution to the radar cross section, while some comparisons between simulated and real SAR images emphasize the possibility of extracting information on the electromagnetic behavior of the objects in the scene. These first interesting results are discussed to comment the efficiency of the deterministic approach and its possible future applications.

Chapter 1

Synthetic Aperture Radar (SAR)

In the last decades a great novelty in the branch of remote sensing, in terms of both new technologies and promising applications, has been represented by the advent and large use of Synthetic Aperture Radar (SAR).

It is able to produce high-resolution images of the Earth's surface, similar to photographic equipment. But a SAR has a number of advantages compared with optical systems: for instance, radar is independent of any illumination by the sun, so that measurements can be made around the clock at any time of day or night. Moreover, a radar sensor is to a large extent independent of weather conditions, such as, for example, cloud coverage. This contributes significantly to the reliability of the system, a property that is increasingly requested by many users, since data are often required at a certain point in time.

Today, these kinds of capabilities are no longer just of interest for scientific applications – such data are also being asked for increasingly on the commercial market.

With the new upcoming SAR satellite, the land masses of the Earth will be particularly closely inspected. This includes the mapping of our forests, the generation and current updating of land utilization maps, the recording of derelict land areas and the estimation of the maturity-level of areas in agricultural use, as well as the study and monitoring of geologically active areas such as volcanic and earthquake regions. With the increasing technical capability of these sensors this kind of data can be extracted from satellites with ever more precision. So, from preventing natural disasters to monitoring the growth of urban centers, the SAR technology has been applied successfully (and will be again) in so many fields that now represents an irreplaceable support for civil protection in all operations of territorial planning and prevention.

In this chapter the rationale and the high performance of this technology in its classical conception are introduced and widely described.

1.1 The Stripmap acquisition mode

The SAR system can image an area over the ground in different operational modes: in the well-known stripmap mode, the radar antenna is pointed along a fixed direction with respect to the platform flight path and the antenna footprint covers a strip on the imaged surface as the platform moves, see Fig.1. Accordingly, the extension of the illuminated area is theoretically unlimited in the along-track (azimuth) direction, but the azimuth resolution cannot be better than a half of the real antenna azimuth length.

Let us evaluate the SAR raw signal for the stripmap mode. At times t_n-$\tau/2$, the sensor radiates pulses represented by:

$$f(t-t_n) = e^{j\omega t} P(t-t_n) rect\left[\frac{t-t_n}{\tau}\right] \tag{1.1}$$

where

$$P(t-t_n) = e^{-j\frac{\alpha}{2}(t-t_n)^2} \tag{1.2}$$

is the chirp impulse, τ is the pulse duration time, $\omega=2\pi f$ with f carrier frequency of the transmitted signal, rect[t/T] is the standard rectangular window function, i.e., rect[t/T]=1 if $|t|\leq T/2$, otherwise rect[t/T]=0.

After a heterodyne process and neglecting inessential amplitude factors, we find that the signal backscattered by a generic point P, see Fig.2, and received by the sensor is:

$$\begin{aligned} f_1(x'-x, t-t_n, r) &= \exp\left(-j\omega\frac{2R}{c}\right)\exp\left(-j\frac{\alpha}{2}\left(t-t_n-\frac{2R}{c}\right)^2\right)\cdot \\ \cdot rect&\left[\frac{t-t_n-2R/c}{\tau}\right]\cdot w^2\left(\frac{x'-x}{X}\right) \end{aligned} \tag{1.3}$$

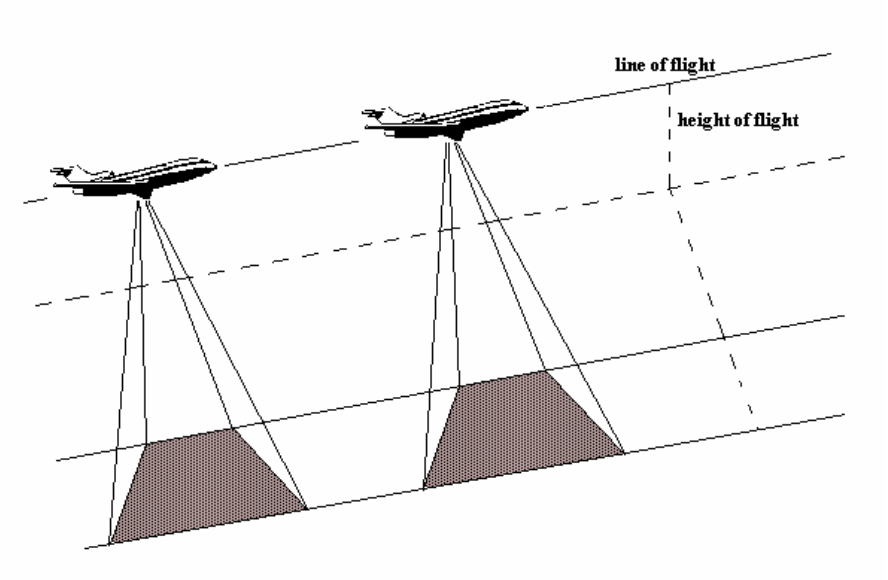

Figure 1 Geometry of the stripmap acquisition mode.

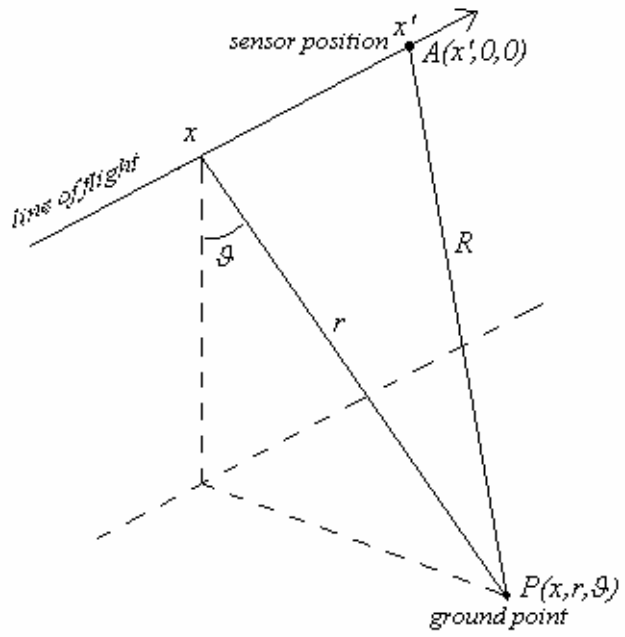

Figure 2 Geometry of the problem.

where x, r, and θ are the coordinates in the cylindrical coordinate system whose axis is the sensor line of flight, $A\equiv(x',0,0)$ is the antenna position, R is the distance from A to the generic point $(x,r,\theta(x,r))$ of the scene, c is the speed of the light, $w(\cdot)$ is the antenna illumination function, related to the azimuth antenna footprint over the ground, $X=\lambda R_0/L_x$ is the real antenna azimuth footprint (we assume that $w(\cdot)$ is negligible when the absolute value of its argument is larger than 1/2, and that it is an even function), λ is the carrier wavelength ($\lambda=c/f$), L_x is the azimuth dimension of the real antenna, R_0 is the distance from the line of flight to the centre of the scene.

The latter term is squared in eq. (1.3) because the same antenna operates also in the receive mode. Equation (1.3) assumes the platforms to move in a *stop and go way*, in the sense that the system is supposed to transmit an to receive the same pulse at the same position: it can be shown [1] that this is a reasonable approximation for all the available SAR systems. From Fig. 2 we have:

$$R=\sqrt{r^2+\left(x'-x\right)^2}=r+\Delta R\,. \tag{1.4}$$

Let us now change the time coordinates in range (spatial) coordinates as follows:

$$r'=\frac{ct'}{2} \tag{1.5}$$

with:

$$t'=t-t_n\,. \tag{1.6}$$

Substituting Eqs(1.4-5) in Eq. (1.3) we have

$$\begin{aligned} f_1\left(x'-x,r'-r,r\right)&=\exp\left(-j\frac{4\pi}{\lambda}r\right)\exp\left(-j\frac{4\pi}{\lambda}\Delta R\right)\cdot\\ \cdot\exp\left(-j\frac{4\pi}{\lambda}\frac{\Delta f/f}{c\tau}\left(r'-r-\Delta R\right)^2\right)&rect\left[\frac{r'-r-\Delta R}{c\tau/2}\right]\cdot w^2\left(\frac{x'-x}{X}\right)\end{aligned} \tag{1.7}$$

where

$$\frac{2\alpha}{c^2} = \frac{4\pi}{\lambda}\frac{\Delta f / f}{c\,\tau} \tag{1.8}$$

with Δf standing for the chirp bandwidth.

Superimposing all the elementary returns from the illuminated surface weighted according the reflectivity $\gamma(x,r)$ [1] of the surface itself we have:

$$\begin{aligned} h_{strip}(x',r') &= \iint \gamma(x,r) f_1(x'-x, r'-r, r)\, dx dr = \\ &= \iint \gamma(x,r) \exp\left(-j\frac{4\pi}{\lambda} r\right) \exp\left(-j\frac{4\pi}{\lambda}\Delta R\right) \cdot \\ &\cdot \exp\left(-j\frac{4\pi}{\lambda}\frac{\Delta f / f}{c\tau}\left(r'-r-\Delta R\right)^2\right) rect\left[\frac{r'-r-\Delta R}{c\tau/2}\right] \cdot w^2\left(\frac{x'-x}{X}\right) \end{aligned} \tag{1.9}$$

Letting

$$\gamma(x,r)\exp\left(-j\frac{4\pi}{\lambda} r\right) \to \gamma(x,r) \tag{1.10}$$

and

$$\begin{aligned} g_{strip}(x'-x,\quad r'-r;\quad r) &= \exp\left[-j\frac{4\pi}{\lambda}\Delta R\right] \cdot \\ \exp\left[-j\frac{4\pi}{\lambda}\frac{\Delta f / f}{c\tau}\left(r'-r-\Delta R\right)^2\right] &\cdot w^2\left(\frac{x'-x}{X}\right) \mathrm{rect}\left[\frac{\left(r'-r-\Delta R\right)}{c\tau/2}\right] \end{aligned} \tag{1.11}$$

we have, in a more compact form,

[1] Hereafter we will assume $\gamma(x',x,r) \approx \gamma(x,r)$. Actually, the reflectivity pattern of still ground point changes as the sensor moves, but the approximation is acceptable for the distances involved.

$$h_{strip}(x',r') = \iint \gamma(x,r)\, g_{strip}(x'-x, r'-r; r)\, dx dr\,, \tag{1.12}$$

with $g_{strip}(\cdot)$ standing for the SAR system impulse response[2].

1.2 SAR Transfer Function

Let us evaluate the *Transfer Function* (TF) of the SAR system, by calculating the 2D Fourier Transform (FT) of the raw data.

By using the stationary phase method it can be shown [1] that the FT of Eq.(1.12) is

$$H_{strip}(\xi,\eta) = \iint \gamma(x,r) G_{strip}(\xi,\eta;r) \exp[-j\xi x] \exp[-j\eta r]\, dx dr \tag{1.13}$$

where

$$\begin{aligned} G_{strip}(\xi,\eta;r) &= \exp\left[j\frac{\eta^2}{4b} \right] \exp\left[j\frac{\xi^2 (r/R_0)}{4a(1+\eta\lambda/(4\pi))} \right] \cdot \\ &\cdot rect\left[\frac{\eta}{2bc\tau/2} \right] w^2\left(\frac{\xi}{2aX} \right) \end{aligned} \tag{1.14}$$

In Eqs. (1.13-14) $H_{strip}()$ and $G_{strip}()$ stand, respectively, for the FT of $h_{strip}()$ and $g_{strip}()$, η and ξ are the frequency domain coordinates corresponding, respectively, to the range and azimuth time domain coordinates and

[2] In Eq.(1.11) a factor rect(x'/X_1) should be added, accounting for the finite length of the considered raw data set. However, in the stripmap case, we always have $X_1 >> X$ and this rect factor can be neglected.

$$a = \frac{2\pi}{\lambda R_0} \tag{1.15}$$

$$b = \frac{4\pi\left(\Delta f / f\right)}{\lambda c \tau} \tag{1.16}$$

Eqs.(1.13-14) represent the starting point for discussing the development of a stripmap SAR raw signal simulator.

1.3 Project supporting tools: a stripmap SAR raw signal simulator

Within the framework of SAR studies, it is convenient to simulate the signal received on board before any processing (with the exception of the heterodyne down-converter), [2]. This is the signal we called *raw* in the previous paragraphs.

Simulation of canonical scenarios may simplify experimentation of processing algorithms, as well as development of pattern recognition and feature extraction techniques. Simulation may play a significant role in studies concerning noise and clutter rejection and may contribute toward optimizing SAR system parameters.

A simulation code must meet a number of stringent constraints. The scenario to be simulated should be rather general and possibly time varying, either deterministically or stochastically. It should rely upon a sound scattering model which must comply with proper statistical rules. An important feature for a SAR simulator of an extended scene is the altitude profile, since the influence of the relief plays a great role in the formation of the final image. Last, but not least, the numerical code should be efficient, fast and (computer) memory saving. These features are usually in competition, and the ultimate solution is generally an engineering compromise.

An example of efficient SAR raw signal simulator for stripmap mode is given in [2].

If we ignore the *r*-dependence of $g_{strip}(\cdot)$, i.e., if we let $r=R_0$ in eq.(1.4), then eq.(1.12) is easily recognised as the 2D convolution between γ and g_{strip}, that can be efficiently performed in the 2D Fourier transformed (FT) domain. Even considering the *r*-dependence, eq.(1.12) can be efficiently computed in the 2D Fourier transformed domain: in fact, by using the

stationary phase method it can be shown [1] that the FT of eq.(1.12) can be write as

$$H_{strip}(\xi,\eta) = G_{0strip}(\xi,\eta)\Gamma[\xi,\eta\Omega(\xi)+\mu(\xi)], \tag{1.17}$$

where again $H_{strip}(\xi,\eta)$ is the FT of $h_{strip}(x,r)$, $\Gamma(\xi,\eta)$ is the FT of $\gamma(x,r)$ and

$$G_{0strip}(\xi,\eta) = \exp\left[j\frac{\eta^2}{4b}\right]\exp\left[j\frac{\xi^2}{4a(1+\eta\lambda/(4\pi))}\right]\mathrm{rect}\left[\frac{\eta}{2bc\tau/2}\right]w^2\left(\frac{\xi}{2aX}\right) \tag{1.18}$$

is the FT of $g_{strip}(x'-x,\ r'-r;\ r=R_0)$, and the functions

$$\mu(\xi) = \frac{\xi^2}{4aR_0}, \qquad \Omega(\xi) = 1-\frac{\xi^2}{4aR_0}\frac{\lambda}{4\pi} \tag{1.19}$$

account for the *r*-space-variant characteristics of the SAR system, i.e., for the *r*-dependence of $g_{strip}(\cdot)$.

Eq.(1.17) suggests that the stripmap SAR raw signal simulation can be performed as shown in the flow chart in Fig.3, where the "Grid Deformation" block performs an interpolation in the Fourier domain, to obtain the desired values $\Gamma[\xi,\eta\Omega(\xi)+\mu(\xi)]$ from the available ones $\Gamma[\xi,\eta]$ (this step can be included in the 2D-FT block by using a chirp scaling algorithm [5,6]).

This is the method employed in the stripmap SAR raw signal simulator presented in [2-4]. Use of efficient FFT algorithms leads, in the case of extended scenes, to a processing time of different orders of magnitude smaller than the one required by a time domain simulation directly based on eqs.(1.11-12).

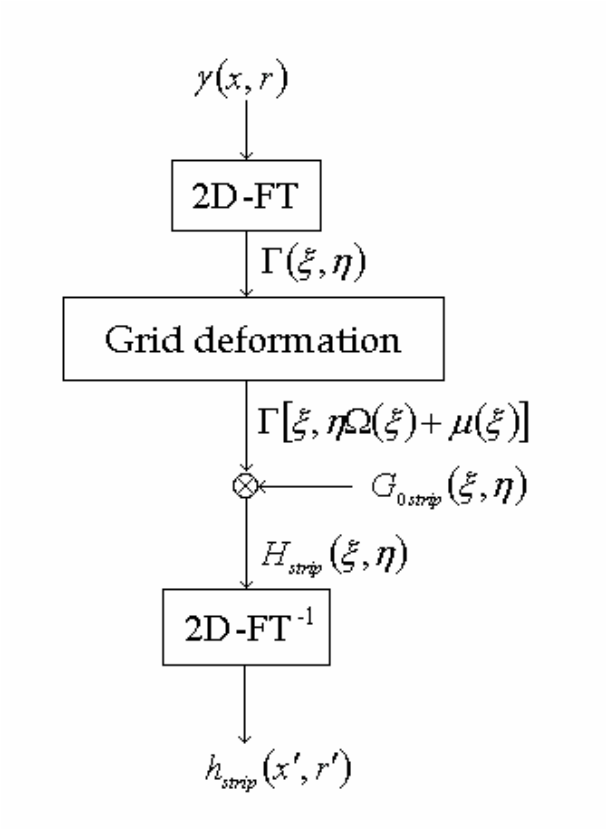

Figure 3 Flow chart of stripmap SAR raw signal simulation.

References

[1] G.Franceschetti and R.Lanari; Synthetic Aperture Radar Processing, CRC PRESS, New York, 1999.

[2] G.Franceschetti, M.Migliaccio, D.Riccio, G.Schirinzi, "SARAS: a SAR raw signal simulator", *IEEE Trans. Geosc. Remote Sensing*, vol.30, pp.110-123, 1992.

[3] G.Franceschetti, M.Migliaccio, D.Riccio, "SAR simulation of actual ground sites described in terms of sparse input data", *IEEE Trans. Geosc. Remote Sensing*, vol.32, pp.1160-1169, 1994.

[4] G.Franceschetti, A.Iodice, M.Migliaccio, D.Riccio, "A Novel Across-Track SAR Interferometry Simulator", *IEEE Trans. Geosc. Remote Sensing*, vol.36, pp.950-962, 1998.

[5] S.Cimmino, G.Franceschetti, A.Iodice, D.Riccio, G.Ruello, "Efficient Spotlight SAR Raw Signal Simulation of Extended Scenes", *IEEE Trans. Geosc. Remote Sensing,* vol.41, pp. 2329- 2337, 2003.

[6] R.K.Raney, H.Runge, R.Bamler, I.G.Cumming, F.H.Wong, "Precision SAR processing using chirp scaling", *IEEE Trans. Geosc. Remote Sensing*, vol.32, pp.786-799, 1994.

Chapter 2

High Resolution SAR

In Chapter 1, the main features of SAR technology have been widely described. The basic concept of spatial resolution has been also introduced thus highlighting one of the most interesting aspects of this kind of remote sensors.

But in the last years the scientific community worked to improve this remarkable radar, in particular thinking of the new and better applications that would have been derived from an advance in the image resolution.

This matter is discussed here.

High Resolution (HR) SAR, in terms of both sensor technology and new spatial missions, is described in this Chapter together with the instruments necessary for its right design, project and use.

2.1 Performance and applications of HR SAR sensors

SAR images with spatial resolution in the order of 1 meter have been always desired but, till today, available only from airborne sensors which involve scanty coverage of the observed area. Such requirements would be much more appealing if satisfied by spaceborne sensors able to produce images of larger areas.

These performances will be soon a reality thanks to the upcoming lunch of a new generation of SAR sensors implementing a technology guaranteeing high spatial resolution [1],[2]. In the last decade a great amount of private and public capital has been invested in research on these topics aiming at the design and realization of HR SAR sensors. The reason for a so general interest lies in the innumerable applications that can be derived. For example, let us think of some basic applications: maps of land use/land cover can provide land surface information on different thematic levels and HR SAR can deliver new input parameters improving existing interpretation methods and thus the quality of these maps. But these sensors will be important supports also of the efficient production and update of Digital

Elevation Models (DEM) describing the relief information of the Earth's surface.

Moreover, HR SARs can support the use of other Earth observation data being capable of providing very detailed information on the observed surface features in an area and, generally, many thematic applications from risk diagnostics to forestry and agriculture mapping will profit by availability of high spatial resolution products as can be better understood looking at an example of HR SAR mission, the German TerraSAR-X, introduced in the following.

2.1.1. The TerraSAR-X mission

TerraSAR-X is Germany's first national remote sensing satellite to be implemented in a public-private partnership between the German Aerospace Center (DLR) and EADS Astrium GmbH, with a significant financial participation from the industrial partner. This radar satellite, which is to be launched at the end of February 2007 using a Russian-Ukrainian launch vehicle, will supply high-quality radar data for purposes of scientific observation of the Earth for a period of at least five years [1],[2]. At the same time it is designed to satisfy the steadily growing demand of the private sector for remote sensing data in the commercial market, thus opening up a self-supporting, sustainable area of business.

From the research point of view the development of techniques and the deepening of knowledge of the factors influencing the environment have high priority. One of the outstanding features of TerraSAR-X is the high spatial resolution that has not previously been achieved by any civilian radar system. This enables the inclusion of detailed ground features for better classification, for example the separation of different types of trees or crops.
But TerraSAR-X will also offer completely new perspectives for the monitoring of urban environments. Around 40% of the people in the developing countries, and over 75% of the people in the industrial nations, live in population centers. Thus with around 3,000 million people approximately half the world's population lives in urban areas. According to latest estimates this proportion will increase over the next three decades to around two thirds. Such a concentration of population is accompanied by an enormous dynamic in terms of alterations in the regions concerned, the results of which are often serious economic, ecological or social conflicts.
In order to be able to detect these potentials for conflict at an early stage and to be able to develop methods for their avoidance and solution, there is a need for a sustainable survey of up-to-date information related to the geographical environment. Today's SAR sensors offer a resolution of about

25 meters that enable the separation of built-up areas from other types of land usage. The high resolution of TerraSAR-X will significantly improve the level of detailing, so that individual buildings, urban layouts and infrastructure, such as streets and railway lines, can be detected and mapped. But the scientific fields of applications for TerraSAR-X are unnumbered. Let us think of the monitoring of the oceans and costal regions, the extent and distribution of sea ice, the tectonic displacement, the volcanic activities and so on.

The public-private partnership agreement arranges for a commercial exploitation of TerraSAR-X data by the industry partner, EADS Astrium GmbH. Apart from the direct financial contribution to the project , the partner is obliged to develop a portfolio of innovative TerraSAR-X-based products and services and to establish a global distribution network. For this purpose, EADS Astrium has founded its 100% subsidiary Infoterra GmbH in 2001.

Infoterra offers TerraSAR-X data in different levels of refinement. They are ranging from Basic Image Products, raw image data that can be acquired in different imaging modes, polarizations and geometric projections according to clients' specifications, to Enhanced Image Products, i.e. orthorectified images or mosaics from several sense, all the way to Geo-information Products, i.e. products that contain significant information such as change detections.

2.2 The spotlight acquisition mode

There are two interesting SAR geometries, both implemented by TerraSAR-X, able to grant high resolution images: the spotlight and the hybrid stripmap/spotlight.

With the spotlight configuration we can improve the stripmap resolution in the azimuth direction (that is $L_x/2$ with L_x standing for the azimuth dimension of the real antenna) by increasing the synthetic aperture extension. The radar antenna beam is steered during the overall acquisition time, see Fig. 1, thus pointing always at the same area over the ground.

This geometry represents the best in terms of azimuth resolution but, obviously, the achieved improvement is traded off by the loss of ground coverage that is now limited while it was unlimited (at least in theory) for the stripmap configuration.

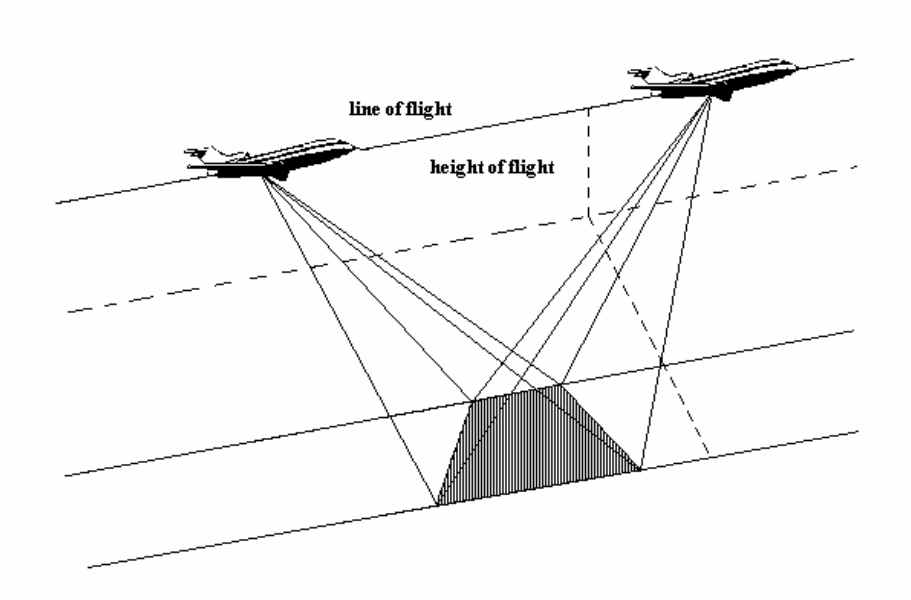

Figure 1 Geometry of the spotlight mode.

2.2.1 Raw signal

In the spotlight mode, the SAR raw signal can be conveniently expressed as follows [3]:

$$h_{spot}(x',r') = \text{rect}\left[\frac{x'}{X_1}\right]\tilde{h}_{spot}(x',r') \tag{2.1}$$

with

$$\tilde{h}_{spot}(x',r') = \iint \gamma(x,r)\, w^2\left(\frac{x}{X}\right) g_{spot}(x'-x,\quad r'-r;\quad r)\,dx\,dr \tag{2.2}$$

and

$$g_{spot}(x'-x,\quad r'-r;\quad r) = \exp\left[-j\frac{4\pi}{\lambda}\Delta R\right]\exp\left[-j\frac{4\pi}{\lambda}\frac{\Delta f/f}{c\tau}\left(r'-r-\Delta R\right)^2\right]\cdot$$

$$\cdot\text{rect}\left[\frac{\left(r'-r-\Delta R\right)}{c\tau/2}\right] \tag{2.3}$$

where X_1 is the length of the trajectory flight portion used to acquire the raw data. Note that, due to the different acquisition geometry, in the spotlight

case the antenna azimuth pattern *w(·)* depends on *x* and not on the difference *x′-x* as in the stripmap case. In addition, Eq. (2.1) includes a rect(·) function of width X_1 accounting for the finite length of the trajectory flight portion used to acquire the raw data.

2.2.2 SAR Transfer Function

By using again the stationary phase method we obtain the following expression for the spotlight raw signal in the frequency domain:

$$H_{spot}(\xi,\eta)=\iint \gamma(x,r)w^2\left(\frac{x}{X}\right)G_{spot}(\xi,\eta;x,r)\exp[-j\xi x]\exp[-j\eta r]dxdr \tag{2.4}$$

where

$$\begin{aligned} G_{spot}(\xi,\eta;x,r)&=\exp\left[j\frac{\eta^2}{4b}\right]\exp\left[j\frac{\xi^2(r/R_0)}{4a\left(1+\eta\lambda/(4\pi)\right)}\right]\cdot \\ &\cdot rect\left[\frac{\eta}{2bc\tau/2}\right]rect\left[\frac{\xi-2ax}{2aX_1}\right] \end{aligned} \tag{2.5}$$

with obvious meaning of the symbols.

2.2.3 Spotlight SAR raw signal simulator

Again, apart from the *r*-dependence of g_{spot}, (that can be managed as in the stripmap case), the integral in Eq. (2.2) is easily recognised as the 2D convolution between $\gamma(x,r)w^2(x/X)$ and g_{spot}, and can be efficiently evaluated in the 2D Fourier transformed domain. In fact, it can be shown that the FT of Eq. (2.2) is [3],[4]:

$$\tilde{H}_{spot}(\xi,\eta)=\tilde{G}_{0spot}(\xi,\eta)\overline{\Gamma}\left(\xi,\eta\Omega(\xi)+\mu(\xi)\right), \tag{2.6}$$

where $\overline{\Gamma}(\xi,\eta)$ is the FT of $\gamma(x,r)w^2(x/X)$ and

$$\tilde{G}_{0spot}(\xi,\eta)=\exp\left[j\frac{\eta^2}{4b}\right]\exp\left[j\frac{\xi^2}{4a\left(1+\eta\lambda/(4\pi)\right)}\right]\cdot \cdot\mathrm{rect}\left[\frac{\eta}{2bc\tau/2}\right]\mathrm{rect}\left[\frac{\xi}{2a\left(X+X_1\right)}\right] \tag{2.7}$$

is the FT of $g_{spot}(x'-x, r'-r; r\equiv R_0)$.

Eqs. (2.6-7) suggest that the spotlight SAR raw signal simulation can be performed as shown in the flow chart in Fig. 2.

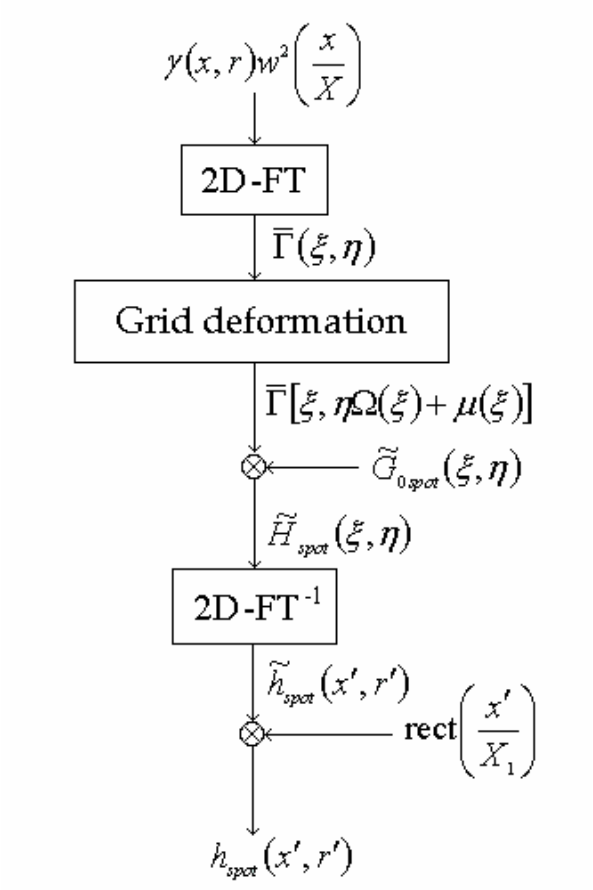

Figure 2 Flow chart of spotlight SAR raw signal simulation.

Above method is the one employed in the spotlight SAR raw signal simulator presented in [3]. In spite of the need for oversampling [3], also in this case use of efficient FFT algorithms leads, in the case of extended scenes, to a processing time of different orders of magnitude smaller than the one required by a time domain simulation directly based on Eqs. (2.1-3).

2.3 The hybrid acquisition mode

Recently, a new operating mode, referred to as hybrid stripmap/spotlight mode, has been presented [5-7]. In the hybrid acquisition the radar antenna beam is steered about a point farther away from the radar than the area being illuminated, see Fig. 3, thus allowing the generation of microwave images with an azimuth resolution better than that achieved in the stripmap configuration, and a ground coverage better than the one of the spotlight configuration.

A number of different processing procedures for hybrid mode have been proposed in the last years [5-8], and, although spaceborne SAR sensors operating in the hybrid mode are not yet available, some are currently under

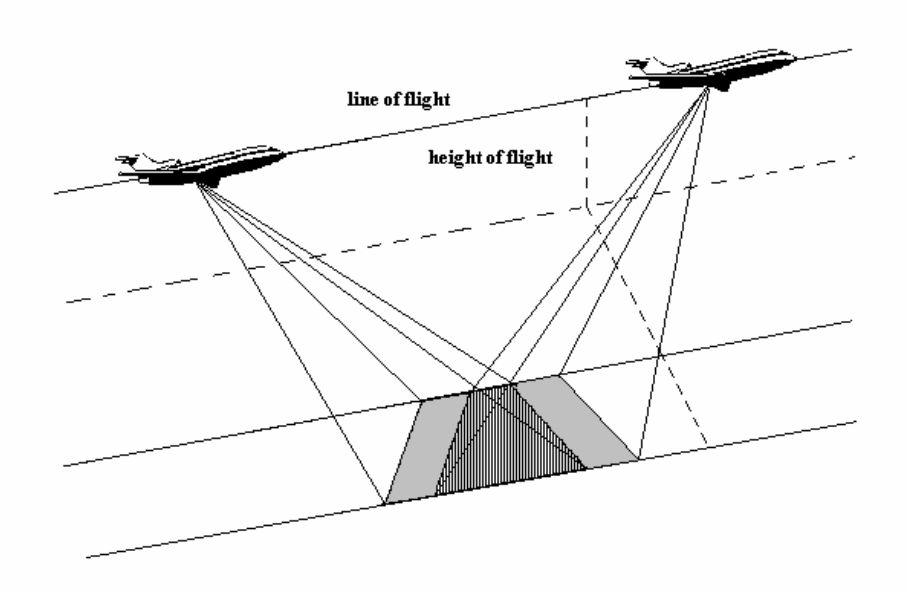

Figure 3 Geometry of the hybrid stripmap/spotlight mode.

design, e.g., SAR 2000 within the Cosmo/Skymed project [9] or TerraSAR-X [1-2]. In addition, airborne SAR sensors implementing hybrid mode are already available, for instance the wideband phased array SAR/MTI system PAMIR [10]. Therefore, the subject of design, processing and data interpretation for the hybrid stripmap/spotlight SAR mode is gaining an increasingly wide interest in the remote sensing scientific community.

To quantitatively support the design of a SAR operating in the hybrid mode, to help mission planning, and to test processing algorithms, a SAR raw signal simulator is required, especially when real raw data are not available yet. In order to test the focusing capability of processing algorithms, point target simulators are usually sufficient. However, it is certainly useful to verify the effect of processing inaccuracies on simulated, and hence perfectly known, extended scenes: in fact, the effects of processing inaccuracies could be "masked" or "emphasised" when complex targets are considered, so that they can vary for different kinds of imaged scenes and hence for different applications. In addition, simulation of SAR raw signals from extended scenes is helpful in SAR system design and mission planning, because it allows to analyse the effects of different design and mission parameter choices for different kinds of imaged scenes. Accordingly, an extended scene SAR raw signal simulator is highly desirable. Such a simulator must include a scattering model and a radar model. The scattering model must evaluate the radar reflectivity as a function of the scene parameters (surface geometry and roughness, permittivity and conductivity) and radar parameters (central frequency, bandwidth, altitude of flight, look-angle, polarisation). The radar model must evaluate the raw signal that would be acquired on board as a function of the radar reflectivity map as well as the sensor operating mode parameters (antenna dimensions, radiation diagrams and azimuthal electronic steering, spacecraft velocity, pulse bandwidth, pulse repetition frequency, sampling frequency).

Time domain SAR raw signal simulation can be easily conceived, but it turns out to be enormously time and memory consuming when extended scenes are considered. The raw signal is represented by a two-fold integral of reflectivity and impulse response function; such integral is not immediately recognised as a convolutional form, and its evaluation must be performed in time domain. This is certainly not efficient, being the sampled reflectivity and impulse response function matrixes of comparable sizes.

Efficient simulators have been presented for the stripmap operational mode [11-13]. There, a frequency domain approach can be followed: a space-variant transfer function is defined and evaluated in closed form; and an overall procedure is presented to efficiently evaluate the raw signal employing this transfer function, FFTs, and an appropriate grid deformation.

We also discussed an efficient simulator recently presented for the spotlight operational mode [14]. Also in this case a frequency domain approach can be followed to simulate the raw signal: an appropriately modified space-variant transfer function is defined and evaluated in closed form; and a different overall procedure is implemented, that employs this modified transfer function, FFTs, appropriate grid deformation, and a simple final time domain multiplication.

Conversely, to the best of our knowledge, no efficient extended scene SAR simulator for the hybrid mode is currently available. Only simple time domain simulators, able to deal with point targets or small scenes, can be found in literature [15-16].

In this chapter efficient time and frequency domain based procedures to simulate the raw signal in the hybrid stripmap/spotlight mode are presented and compared. To address this item, a new transfer function is defined. We show that in this case a 2D Fourier domain approach is not viable. However, we demonstrate that a 1D range Fourier domain approach, followed by 1D azimuth time domain integration, is possible, if we accept some approximations usually valid in the actual cases. We show that this method is still much more efficient than the time domain one, so that extended scenes can be considered.

2.3.1 Raw signal

In order to evaluate the SAR raw signal for the hybrid configuration, we have to introduce the factor [5-7]

$$A = \frac{r_1}{r_1 + R_0}, \tag{2.8}$$

where R_0 is the distance from the line of flight to the centre of the scene and r_1 is the distance from the ground to the beam steering point position beneath, so that r_1+R_0 is the distance from the line of flight to the steering point position, see Fig. 4.

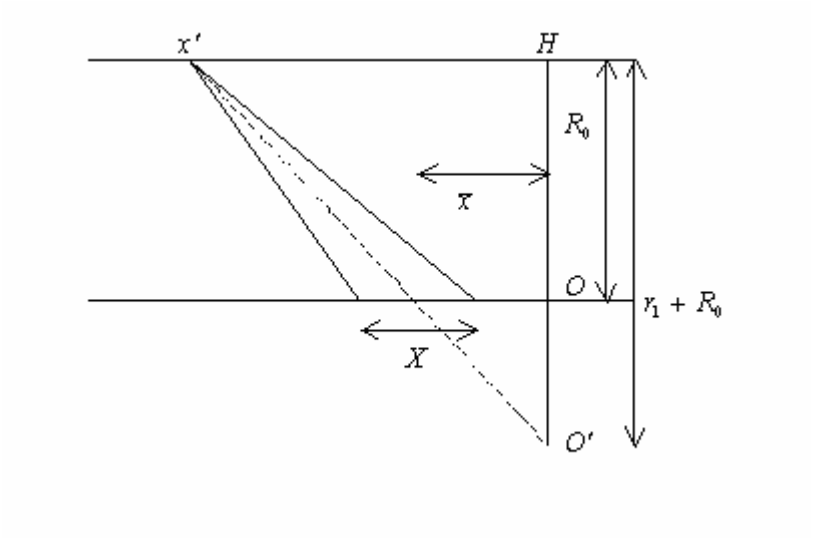

Figure 4 Hybrid stripmap/spotlight mode: illuminated area.

It can be shown [7] that use of the hybrid configuration is convenient when $2X/X_1<A<1$, and that in this case the resolution is increased by a factor $1/A$ with respect to the stripmap case, whereas the fully resolved covered area is increased by a factor $A(X_1/X)$-1 with respect to the spotlight case.

From the system geometry depicted in Fig. 4 it is evident that, by steering the antenna about infinity (A=1) or about the scene centre (A=0), stripmap or spotlight configurations are obtained, respectively. In the intermediate cases ($0<A<1$), for a given sensor position x' the illuminated area is centred around a point with azimuth coordinate $\bar{x} = Ax'$ and has an azimuth size equal to X, see Fig. 4. Accordingly, the azimuth illumination diagram of the real antenna is of the form

$$w\left(\frac{Ax'-x}{X}\right), \tag{2.9}$$

that leads to the expression of the hybrid SAR raw signal given below:

$$h_{hybrid}(x',r') = \iint \gamma(x,r) g_{hybrid}(x'-x, r'-r; x, r)\,dx\,dr\,, \tag{2.10}$$

where

$$g_{hybrid}(x'-x,r'-r;x,r)=\exp\left[-j\frac{4\pi}{\lambda}\Delta R\right]\exp\left[-j\frac{4\pi}{\lambda}\frac{\Delta f/f}{c\tau}\left(r'-r-\Delta R\right)^2\right]\cdot$$
$$\cdot w^2\left(\frac{Ax'-x}{X}\right)\mathrm{rect}\left[\frac{x'}{X_1}\right]\mathrm{rect}\left[\frac{\left(r'-r-\Delta R\right)}{c\tau/2}\right] \tag{2.11}$$

As expected, in the limiting cases A=1 and A=0, Eqs. (2.10-11) reduce to the expression of the SAR raw signal in the stripmap and spotlight acquisition modes, respectively. Unfortunately, in the intermediate cases ($0<A<1$) the integral in Eq. (2.10) cannot be expressed as a 2D convolution, and cannot be efficiently evaluated in the 2D Fourier transformed domain as detailed in the next paragraph.

2.3.2 SAR Transfer Function

A stationary phase evaluation of the FT of Eq. (2.10) along the same guideline of the stripmap and spotlight cases [4] leads to

$$H_{hybrid}(\xi,\eta)=\iint\gamma(x,r)G_{hybrid}(\xi,\eta;x,r)\exp[-j\xi x]\exp[-j\eta r]dxdr\,, \tag{2.12}$$

where

$$G_{hybrid}(\xi,\eta;x,r)=\exp\left[j\frac{\eta^2}{4b}\right]\exp\left[j\frac{\xi^2\left(r/R_0\right)}{4a\left(1+\eta\lambda/(4\pi)\right)}\right]\cdot$$
$$\cdot\mathrm{rect}\left[\frac{\eta}{2bc\tau/2}\right]\mathrm{rect}\left[\frac{\xi-2ax}{2aX_1}\right]w^2\left[\frac{\xi-2a\left(1-1/A\right)x}{2aX/A}\right] \tag{2.13}$$

Examination of Eqs. (2.12-13), shows that, at variance of previous cases, a two-fold integration is needed. The r-integration can be dominated by expanding the second exponential in Eq. (2.13) as it is done in the strip and in the spot cases. The result would be a more involved functional dependence of the FT of $\gamma(x,r)$. But no similar procedure can be implemented for the x-dependence and an efficient simulation algorithm cannot be devised in this domain. On the other hand, an algorithm in the space domain, directly based on Eq. (2.10), even if always possible in theory, is not computationally efficient, and hence not usable in practice if

extended scenes are considered. An alternative approach, involving 1D range FT's, is described in the following paragraph.

2.4 Efficient simulation of hybrid SAR raw signal

2.4.1 Rationale

Let us use the exact value of ΔR in the first exponential of Eq. (2.11), but let us approximate ΔR with its value at the scene centre (i.e., at $r = R_0$) in the second exponential: in such a way, the most important part of the range space-variance is accounted for, and only the effect of space variance on range curvature [4] is neglected. This is usually an acceptable approximation, as shown in Appendix. If this is not the case, the range swath can be subdivided in different subswaths, for each of which above approximation holds, see the Appendix. By proceeding with this approximation, the hybrid SAR raw signal can be expressed as follows:

$$h_{hybrid}(x',r') \cong \int dx w^2\left[\frac{Ax'-x}{X}\right]\mathrm{rect}\left[\frac{x'}{X_1}\right]\left\{\int dr\gamma_1(x'-x,x,r)\,g(x'-x,r'-r)\right\} \tag{2.14}$$

where

$$\gamma_1(x'-x,x,r) = \gamma(x,r)\exp\left[-j\frac{4\pi}{\lambda}\Delta R\right], \tag{2.15}$$

$$g(x'-x,r'-r) = \exp\left[-j\frac{4\pi}{\lambda}\frac{\Delta f/f}{c\tau}(r'-r-\Delta R_0)^2\right]rect\left[\frac{r'-r-\Delta R_0}{c\tau/2}\right] \tag{2.16}$$

and

$$\Delta R_0 = \Delta R(r=R_0) = \sqrt{R_0^2+(x'-x)^2} - R_0, \tag{2.17}$$

thus separating the terms depending only on azimuth coordinate from those depending on both azimuth and range ones.

In Eq. (2.14), the last term in the graph parentheses is recognized as the range-convolution between $\gamma_1(x'-x,x,r)$ and $g(x'-x,r)$. Therefore, Eq. (2.14) can be also written as:

$$h_{hybrid}(x',r') = \int dx w^2\left[\frac{Ax'-x}{X}\right]\mathrm{rect}\left[\frac{x'}{X_1}\right]\cdot\left\{\Im^{-1}\left[\Gamma_1(x'-x,x,\eta)\cdot G(x'-x,\eta)\right]\right\} \tag{2.18}$$

where $\Gamma_1(x'-x,x,\eta)$ and $G(x'-x,\eta)$ are the 1D range FT of $\gamma_1(x'-x,x,r)$ and $g(x'-x,r)$ respectively:

$$\Gamma_1(x'-x,x,\eta) = \int dr\gamma_1(x'-x,x,r)\exp(-j\eta r)\,, \tag{2.19}$$

$$G(x'-x,\eta) = \int dr\exp\left[-j\frac{4\pi}{\lambda}\frac{\Delta f/f}{c\tau}(r-\Delta R_0)^2\right]\mathrm{rect}\left[\frac{(r-\Delta R_0)}{c\tau/2}\right]\exp(-j\eta r) \tag{2.20}$$

and $\Im^{-1}$ stands for "inverse FT".

Analytical evaluation of Eq. (2.20) is now in order. Letting:

$$q = r - \Delta R_0 \tag{2.21}$$

and

$$\Psi(q) = \eta q + \frac{4\pi}{\lambda}\frac{\Delta f/f}{c\tau}q^2\ , \tag{2.22}$$

Eq. (2.20) becomes:

$$G(x'-x,\eta) = \exp(-j\eta\Delta R_0)\int \mathrm{rect}\left[\frac{q}{c\tau/2}\right]\exp\left[-j\Psi(q)\right]dq\,. \tag{2.23}$$

Normalization of q to $c\tau/2$ shows that stationary phase asymptotic evaluation of Eq. (2.23) is appropriate if $2\pi\Delta f\cdot\tau$ is large, as it is the case for all SAR systems. The stationary phase point q_s is solution of the equation

$$\left.\frac{\partial\psi}{\partial q}\right|_{q=q_s} = \eta + 2\frac{4\pi(\Delta f/f)}{\lambda c\tau}q_s = 0\,, \tag{2.24}$$

i.e., $q_s = -\frac{\eta}{2b}$ (2.25)

and we get

$$G(x'-x,\eta) \approx \exp(-j\eta\Delta R_0)\exp\left[j\frac{\eta^2}{4b}\right]\mathrm{rect}\left[\frac{\eta}{2bc\tau/2}\right]. \quad (2.26)$$

where the parameter b is given in Eq. (1.16).

Eqs. (2.18, 2.26) suggest that the hybrid SAR raw signal simulation can be performed via the following steps (see Fig. 5):

- generation of the scene reflectivity pattern $\gamma(x,r)$. This step is performed exactly in the same way as in the case of the stripmap mode: the scene surface is subdivided in facets smaller than the final system resolution, but much larger than wavelength; for each facet, the scattering coefficient is generated as a complex circular Gaussian random variable (characterised by Rayleigh amplitude and uniform phase distribution), whose variance is computed by considering incidence angle, polarisation, and facet's roughness, conductivity and permittivity, see Refs.[11-12] for details;

- for each x':
  - multiplication of $\gamma(x,r)$ by $\exp\left[-j\frac{4\pi}{\lambda}\Delta R\right]$ to obtain $\gamma_1(x'-x,x,r)$;
  - implementation of 1D FFT of $\gamma_1(x'-x,x,r)$ to obtain $\Gamma_1(x'-x,x,\eta)$;
  - multiplication by $G(x'-x,\eta)$;
  - implementation of 1D inverse FFT to get $\Im^{-1}\left[\Gamma_1(x'-x,x,\eta)\cdot G(x'-x,\eta)\right]$;
  - multiplication by $w^2\left[\frac{Ax'-x}{X}\right]$;
  - integration over x;
- multiplication by $\mathrm{rect}\left[\frac{x'}{X_1}\right]$.

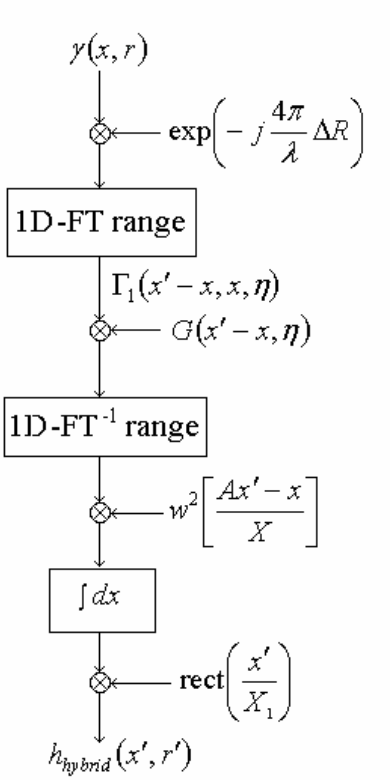

Figure 5 Flow chart of hybrid stripmap/spotlight SAR raw signal simulation. All the steps must be iterated for each value of x'.

This is the method employed in the simulator proposed here.

It must be noted that presented procedure assumes a straight line flight path. This is usually a good approximation for a few kilometres portion of the elliptical orbit of a spaceborne sensor. Conversely, in the case of airborne sensors appreciable deviations from the ideal trajectory may occur: effects of these deviations can be easily accounted for by our simulation scheme, since the azimuth processing is performed in time domain. Accordingly, it is sufficient to let in Eqs. (2.11,15,17)

$$\Delta R = \Delta R(x'-x;r) = R - r = \sqrt{[r+\Delta r(x')]^2 + (x'-x)^2} - r \quad , \quad (2.27)$$

where $\Delta r(x')$ is the projection along the line of sight of the deviation with respect to the nominal trajectory at the sensor azimuth location x'.

2.4.2 Computational complexity

It is now appropriate to compare the computational complexity of the proposed algorithm to the one of a full time domain direct approach. In this analysis we do not consider generation of the reflectivity map, which is the same in both approaches.

If the hybrid raw signal is evaluated in time domain directly from Eq. (2.10), the efficiency of FFT codes is not exploited, and the computational complexity is:

$$N_{TD} \approx \left(N_x N_r\right)^2, \tag{2.28}$$

wherein N_{TD} is the required number of complex multiplications and N_x, N_r are the azimuth and range dimensions (in pixels) of the final hybrid raw signal, respectively (we are assuming that the number of scene facets is of the same order of the number of raw signal pixels).

As for the Fourier approach, the 1D range FFT of $\gamma_1\left(x'-x,x,r\right)$ is calculated for each couple of values *(x',x)* so this step exhibits the computational complexity:

$$N_x{}^2 \frac{N_r}{2} \log_2 N_r . \tag{2.29}$$

At this point the matrix $\Gamma_1\left(x'-x,x,\eta\right)$ is multiplied by the function $G\left(x'-x,\eta\right)$ for every value $\left(x',x,\eta\right)$ and then the inverse 1D range FFT of the updated matrix is evaluated. This stage exhibits the computational complexity:

$$N_x{}^2 N_r + N_x{}^2 \frac{N_r}{2} \log_2 N . \tag{2.30}$$

Therefore, the overall computational complexity of the above described algorithm is:

$$N_H = N_x{}^2 N_r \left(1+\log_2 N_r\right), \tag{2.31}$$

wherein N_H is the number of complex multiplications. Accordingly, by using the suggested hybrid time-Fourier domain approach, processing time is reduced by the factor

$$\frac{N_H}{N_{TD}} = \frac{N_x{}^2 N_r \left(1+\log_2 N_r\right)}{N_x{}^2 N_r{}^2} = \frac{1+\log_2 N_r}{N_r} \tag{2.32}$$

with respect to a time domain simulation. For a 4096x4096 hybrid raw signal we obtain a processing time decrease factor of about 1/315.

2.4.3 Simulation examples

Generation and examination of simulated data is necessary to test the effectiveness of the hybrid raw signal simulator. First of all, we want to verify that the raw signal corresponding to a single scattering point, simulated by using the proposed hybrid time-Fourier domain approach, is in agreement with the one obtained directly from the exact time domain expression, i.e., Eq. (2.10) where the reflectivity map $\gamma(\cdot)$ is a Dirac pulse, so that no integration is needed.

We refer to a hypothetical hybrid spaceborne sensor, whose parameters are reported in Table I, third column. We simulate the raw signal of a point scatterer placed at the centre of the illuminated scene (i.e., the coordinates of the point scatterer are $x = 0$, $r = R_0$). First, phase error is considered, i.e., the phase difference between the raw signal simulated by using the proposed approach and the one obtained via full time-domain simulation: the results are shown in the plots of Fig. 6 for given values of A and $Q = X_1/X$.

Table I
Main SAR system data used in the simulation runs.

Figure Number	8	6-7-10-12
Platform height (h)	5.7 km	775 km
Platform velocity (v)	0.08176 km/s	6.69 km/s
Look angle (θ)	40 degrees	23 degrees
Azimuth antenna dimension (L)	1.0 m	15.0 m
Range antenna dimension	0.12 m	6.0 m
Carrier frequency (f)	9.6 GHz	5.3 GHz
Pulse duration (τ)	5 μs	55 μs
Pulse bandwidth (Δf)	100 MHz	70 MHz
Sampling frequency (f_c)	100 MHz	100 MHz
Pulse repetition frequency (PRF)	300 Hz	900 Hz
A	0.80	0.50
Q	3	6

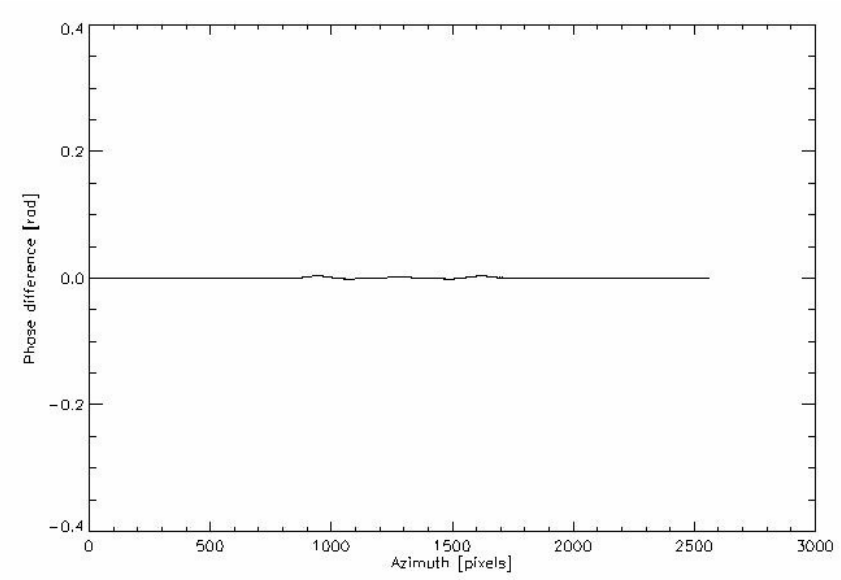

(a)

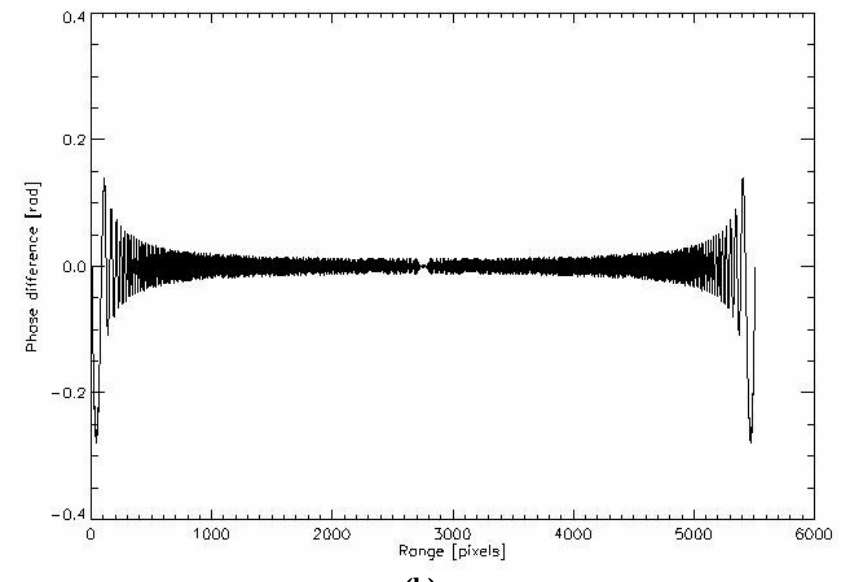

(b)

Figure 6 Difference between the phase of the raw signal simulated by using the proposed approach and the phase of the raw signal obtained by time domain simulation: (a) azimuth cut; (b) range cut. A=0.50, Q=6. The scattering point is placed in the centre of the illuminated scene.

In particular, in Fig. 6a the plot of a cut of this phase difference along the azimuth direction is reported, whereas in Fig. 6b the plot of a cut of the same phase difference along the range direction is shown. It can be noted that the absolute value of this phase difference is always smaller, and often much smaller, than $\pi/10$, thus leading to negligible effects.

Raw signal amplitudes are considered in Fig. 7, where azimuth and range cuts of the amplitude of the raw signal obtained by the proposed approach and by using Eq. (2.10) are reported. Only small oscillations around the exact constant value can be noted.

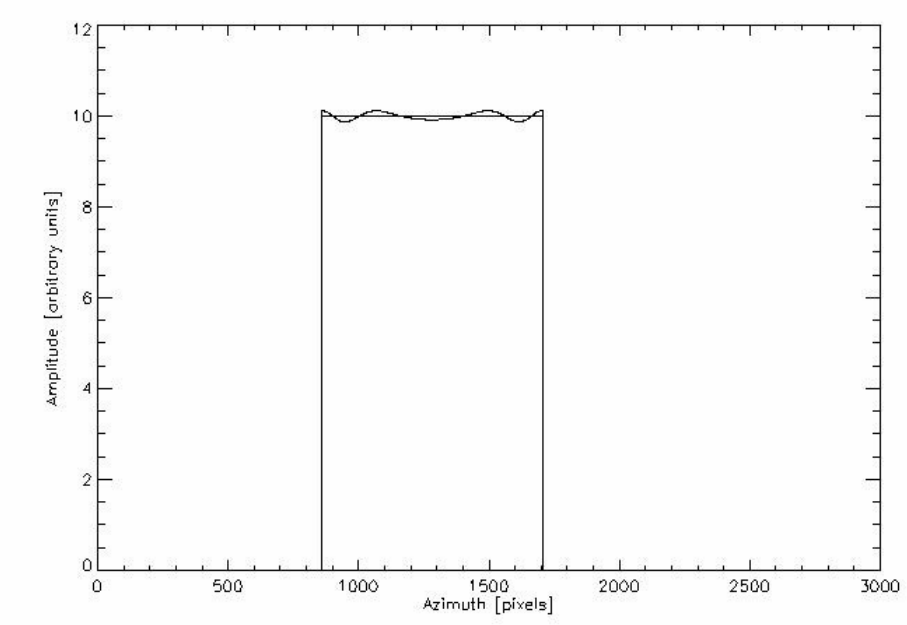

(a)

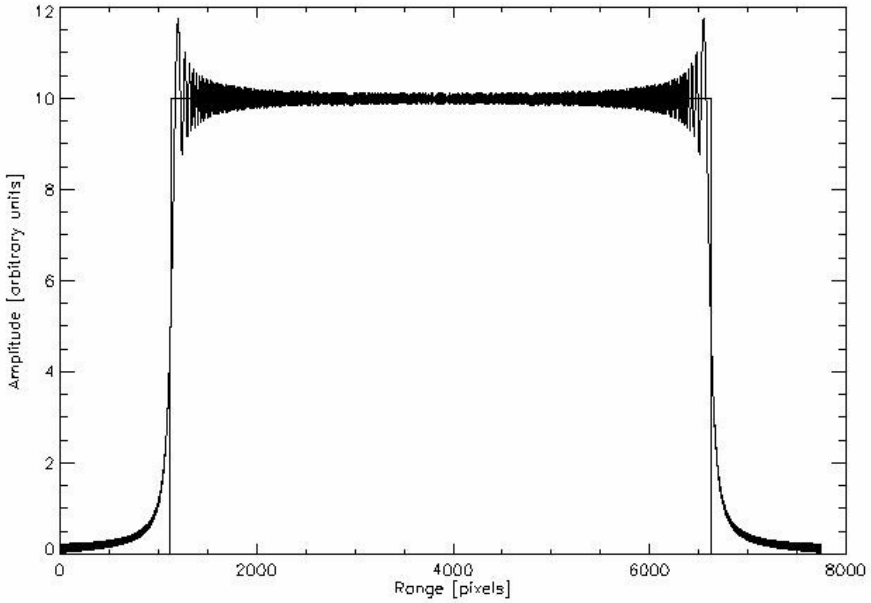

(b)

Figure 7 Amplitudes of the raw signals simulated by using the proposed approach (oscillating curve) and obtained by time domain simulation (straight line): (a) azimuth cut; (b) range cut. A=0.50, Q=6.

Similar comparisons for a point scatterer located at the azimuth and at the range borders of the illuminated area and for different values of the factors A and Q provide very similar results: the error is essentially the same, thus validating the proposed approach.

An airborne case (see Table I, second column) with instable trajectory is now analysed. By using the approach described at the end of §2.4.1 we can deal with extended scenes and arbitrary trajectory deviations. However, we here consider a scattering point located at the centre of the illuminated scene and sinusoidal deviations with respect to the ideal trajectory. In fact, in this case the effect of trajectory instability on the final image can be theoretically predicted [17], and it consists of the appearance of replicas weighted by factors related to Bessel functions and with a spatial separation related to the spatial period P of the sinusoidal deviation. More precisely, the spatial separation is expected to be [17]

$$Dx = (L/2)(X/P) \; . \qquad (2.33)$$

In our simulation the trajectory sinusoidal deviation has a 1 cm amplitude and a 11.6 m period. In Fig.8 an azimuth cut of the image obtained by processing the simulated raw signal with no motion compensation is shown. As expected, a number of weighted replicas of the point target appear. The minimum visible spacing in Fig. 8 is about 36 pixels, which, multiplied by the azimuth pixel spacing (0.28 m), gives a 10 m spacing. This value is in agreement with the expected one, obtained by using in Eq. (2.33) the airborne system data of Table I (X=232.5 m, L=1 m) and P = 11.6 m.

Simulations relevant to extended scenes are now in order. We consider the same spaceborne SAR system data of Table I, third column, and a

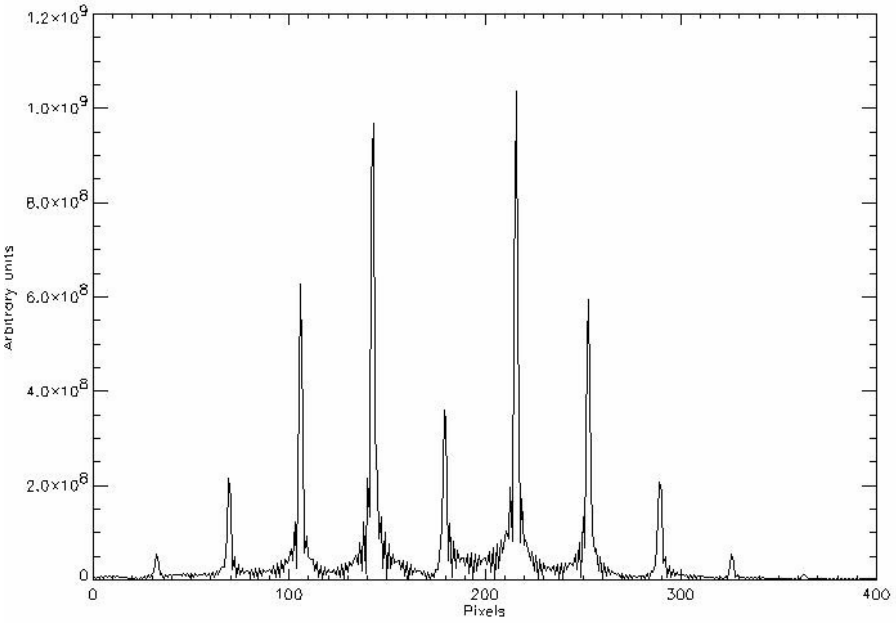

Figure 8 Azimuth cut of the image obtained by processing the simulated raw signal relative to an airborne SAR system with sinusoidal trajectory deviation (amplitude = 1 cm, period = 11.6 m). A=0.80, Q=3. The scattering point is placed in the centre of the illuminated scene.

"canonical" extended scene: a cone over a flat plane, see Fig. 9. In the following experiments, we assume that outside the fully resolved area the scene is perfectly absorbing. Corresponding raw signal has been generated.

In Fig. 10a we show the image that can be obtained by using a hybrid focusing algorithm, whereas in Fig. 10b we show the image obtained by processing the simulated raw signals with a Fourier domain focusing algorithm conceived for stripmap raw signals. In both cases, near range is on the left.

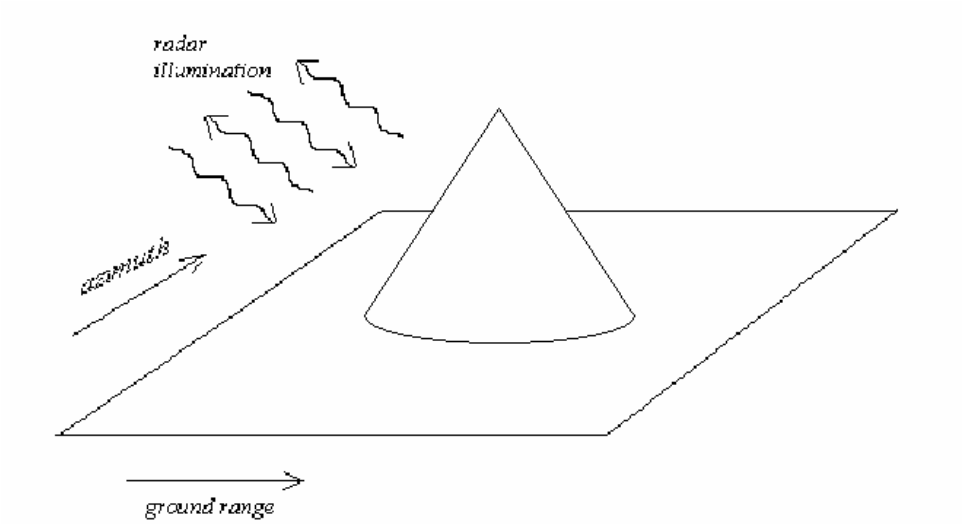

Figure 9 A "canonical" extended scene: a cone over a plane.

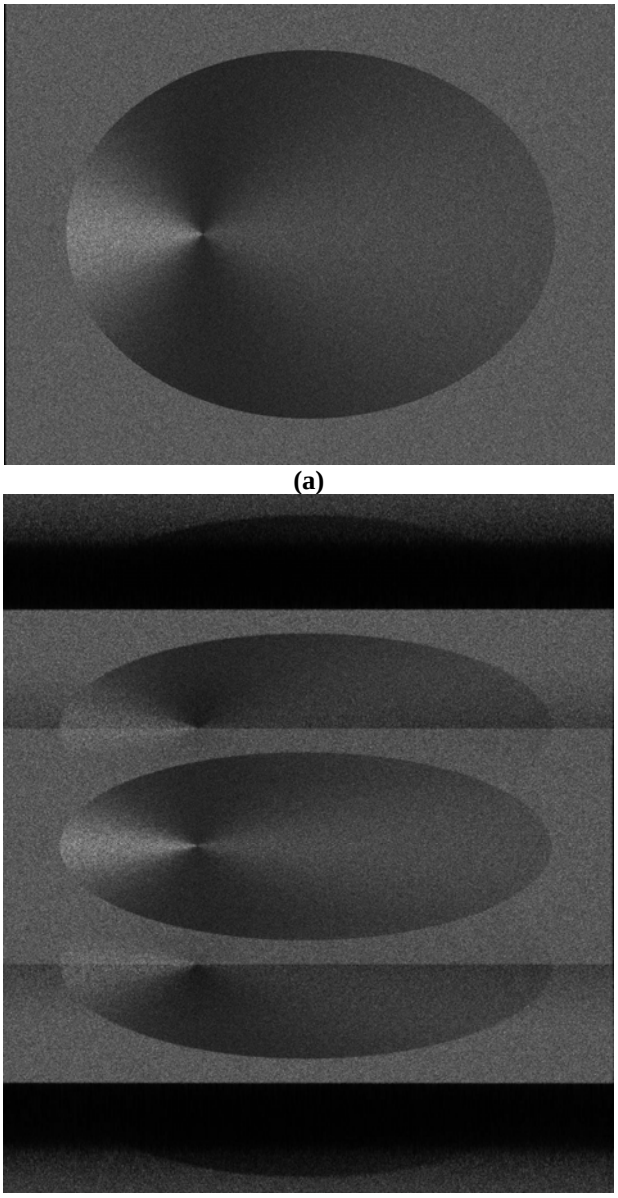

(a)

(b)

Figure 10 Image of a cone over a plane, obtained by (a) ideal hybrid processing, and (b) by processing the simulated hybrid SAR raw signal via a Fourier domain stripmap focusing algorithm. Near range is on the left. A=0.50, Q=6. Azimuth spectrum folding effect is evident in (b). In Fig. (a) the azimuth extension of the scene appears greater than the one of Fig. (b) because of the better resolution of the hybrid mode that leads to a larger number of pixels.

Table II
Main scene data relevant to Figs. 6-12

Figure Number	8	6-7-10-12
Azimuth dimension of the scene (km)	0.3	6.4
Ground range dimension of the scene (km)	1.3	8.6
Azimuth resolution (m)	0.4	3.8
Ground range resolution (m)	2.3	3.8
Raw signal azimuth size (pixels)	2560	2565
Raw signal range size (pixels)	1048	7750

Data relevant to Fig. 10 are reported in Table II, third column. Note that in Fig 10b the azimuth spectrum folding effect, due to the fact that the azimuth raw signal bandwidth is greater than the PRF, causes the appearance of some replicas of the imaged scene, since a Fourier Domain stripmap focusing algorithm has been used. This is in agreement with what happens for real hybrid data. The upper and lower replicas, related to the azimuth borders of the raw signal, exhibit dark areas due to the fact that outside the fully resolved area the scene is perfectly absorbing.

Finally, we consider an actual complex extended scene, given by the Digital Elevation Model of the area of Maratea, Italy, see Fig. 11.

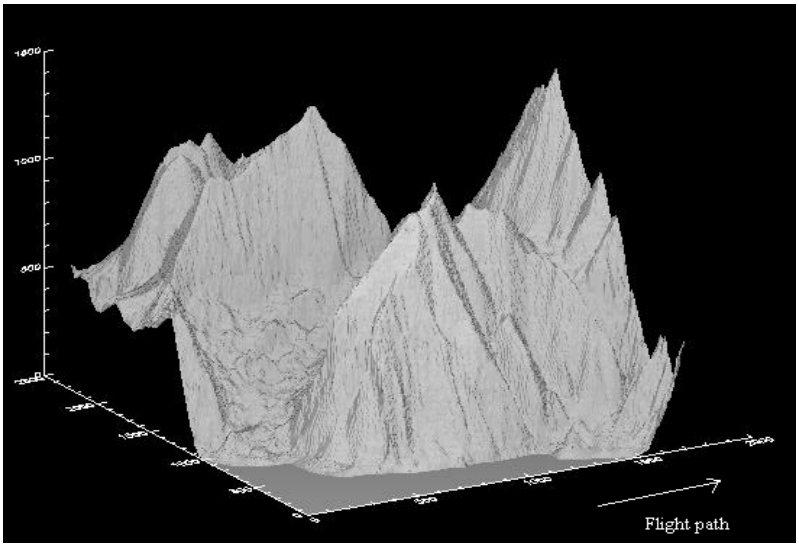

Figure 11 An "actual" extended scene: the Digital Elevation Model of the area of Maratea, Italy.

Corresponding raw signal has been generated with the same system parameters of Figs.9-10. The final images are shown in Fig. 12 according to the same format of Fig. 10. Considerations analogous to those reported for Fig. 10 can be repeated for Fig. 12, but in Fig. 12b the effects of inappropriate processing are dramatically emphasized in this more complex scene.

A few last words are now due about processing times. Obviously, each raw signal simulation required a processing time depending on the chosen system parameters (Table I) and couple (A,Q). In any case, for scenes of the order of some thousands by some thousands pixels, processing time is of the order of several hours. For instance, for a scene of 3650x3650 samples, the raw signal simulation took about eleven hours on a Pentium 4 – 2.00 GHz PC. Note that time domain processing for the same scene would require a processing time of the order of months.

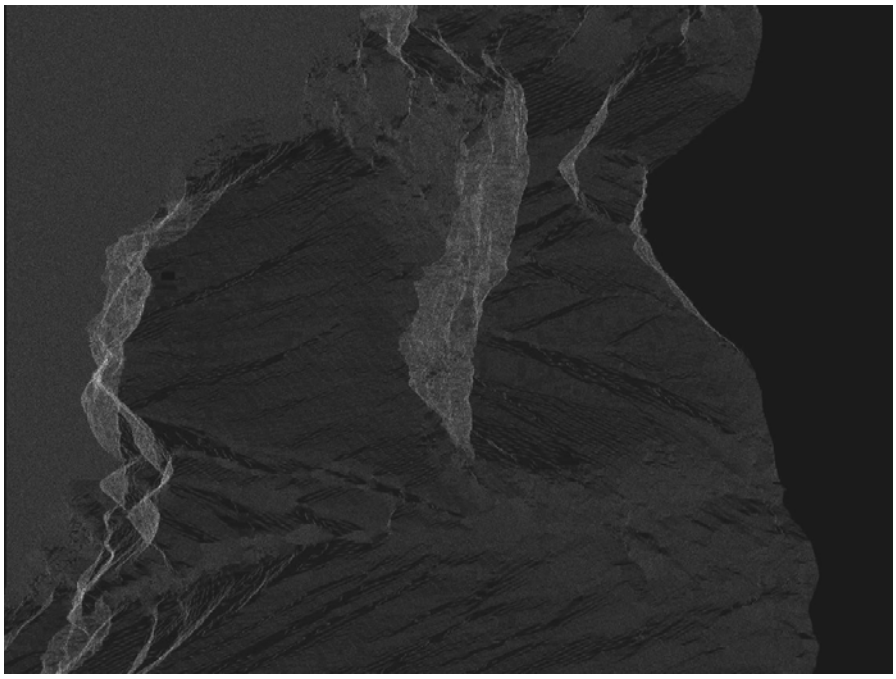

(a)

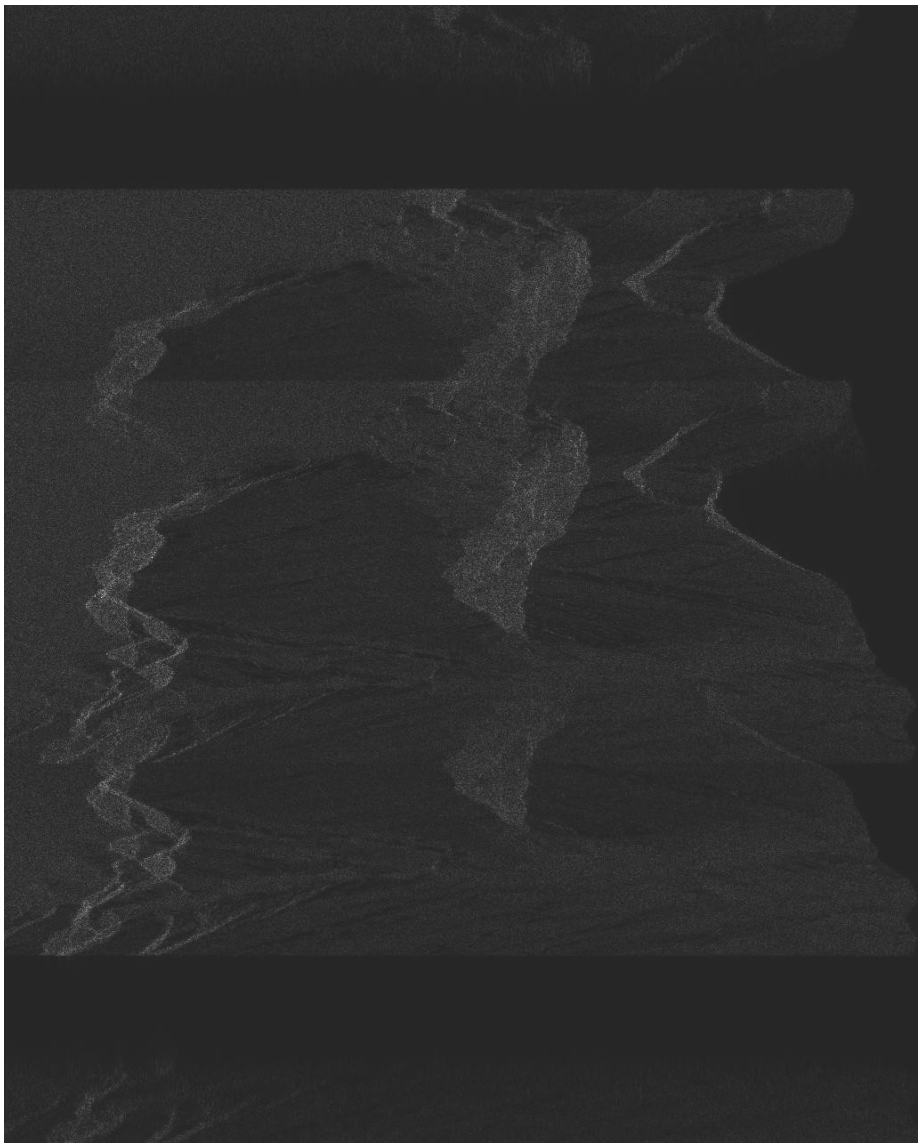

(b)

Figure 12 Image of an actual complex scene (Maratea), obtained by (a) ideal hybrid processing, and (b) by processing the simulated hybrid SAR raw signal via a Fourier domain stripmap focusing algorithm. Near range is on the left. A=0.50, Q=6. Azimuth spectrum folding effect is evident in (b).

APPENDIX

In this Appendix we determine the conditions under which the approximation involved in Eq. (2.14) holds, i.e.,

$$\exp\left[-j\frac{4\pi}{\lambda}\frac{\Delta f/f}{c\tau}\left(r'-r-\Delta R\right)^2\right]\cong\exp\left[-j\frac{4\pi}{\lambda}\frac{\Delta f/f}{c\tau}\left(r'-r-\Delta R_0\right)^2\right], \tag{A.1}$$

where ΔR_0 is given by Eq. (2.17).

First of all, we note that

$$\left(r'-r-\Delta R\right)^2=\left(r'-r-\Delta R_0\right)^2-2(r'-r-\Delta R_0)\left(\Delta R-\Delta R_0\right)+\left(\Delta R-\Delta R_0\right)^2=$$
$$=\left(r'-r-\Delta R_0\right)^2-2(r'-r-\Delta\bar{R})\left(\Delta R-\Delta R_0\right) \tag{A.2}$$

with $\Delta\bar{R}=\left(\Delta R+\Delta R_0\right)/2$. Accordingly, Eq. (A.1) holds if

$$\frac{4\pi}{\lambda}\frac{\Delta f/f}{c\tau}2(r'-r-\Delta\bar{R})\left(\Delta R-\Delta R_0\right)<<1\ . \tag{A.3}$$

In practice, it is sufficient that above quantity is smaller than $\pi/4$ in the worst case (i.e., in near or far range).

Computation of upper bounds for the two factors appearing in Eq. (A.3) is in order.

For the first we have $(r'-r-\Delta\bar{R})\cong(r'-r-\Delta R)\le c\tau/2$. For the second

$$\Delta R-\Delta R_0\cong\frac{\left(x'-x\right)^2}{2r}-\frac{\left(x'-x\right)^2}{2R_0}=\frac{\left(x'-x\right)^2}{2R_0}\left(\frac{R_0}{r}-1\right)\cong-\frac{\left(x'-x\right)^2}{2{R_0}^2}\left(r-R_0\right) \tag{A.4}$$

and

$$\left|x'-x\right|\le\frac{X_1-X_F}{2}\ , \tag{A.5}$$

$$\left|r-R_0\right|\le\frac{S}{2}\ , \tag{A.6}$$

where $X_F=AX_I-X$ is azimuth size of the fully resolved zone [7] and S is the (slant) range extension of the imaged area. It follows that

$$\Delta R - \Delta R_0 \le \frac{\left(X_1 - X_F\right)^2}{2R_0{}^2 \cdot 4} \cdot \frac{S}{2} = \frac{1}{8}\left(\frac{X_1 - X_F}{R_0}\right)^2 \cdot \frac{S}{2} \qquad \text{(A.7)}$$

The final result is

$$\frac{4\pi}{\lambda}\frac{\Delta f / f}{c\tau} 2(r' - r - \Delta\bar{R})\left(\Delta R - \Delta R_0\right) \le \frac{\pi\Delta f}{c}\frac{1}{2}\left(\frac{X_1 - X_F}{R_0}\right)^2 \cdot \frac{S}{2} \quad . \qquad \text{(A.8)}$$

The factor $\pi\Delta f / (2c)$ is usually of the order of 10^{-1}, approaching 1 only for very high range resolution systems (of the order of 1 m). The ratio in parenthesis is of the order of a few times 10^{-2}, so that its square is of the order of $10^{-3} \div 10^{-4}$. Accordingly, even in the case of very high range resolution a range swath of the order of a few km is allowed. For instance, for an hypothetic high resolution spaceborne SAR system with λ=3 cm, L= 6 m, R_0=1000 km (so that X=5 km), Δf=150 MHz, X_1=30 km, and A=0.5 we have:

$$\frac{\pi\Delta f}{c}\frac{1}{2}\left(\frac{X_1 - X_F}{R_0}\right)^2 = \frac{\pi}{4} \cdot \frac{1}{2500} \text{ m}^{-1} \ ,$$

so that a range swath of about 5 km is allowed. Considering that in this case the azimuth size of the fully resolved scene is X_F = 10 km, the obtained range swath is realistic. In any case, a wider range swath of 10 km can be simulated by generating separately the raw signals from two adjacent range swaths and properly summing them.

References

[1] M. Suess, S.Riegger, W.Pitz, R.Werninghaus, "TERRASAR-X – Design and Performance", *Proc. Of EUSAR2002,* Koln, Germany, 2002.

[2] J.Mittermayer, V.Alberga, S.Buckreuβ, S.Riegger, "TerraSAR-X: Predicted Performance", *Proc. SPIE – Int. Soc. Opt. Eng.*, vol.4881, Crete, Greece, 2002.

[3] S.Cimmino, G.Franceschetti, A.Iodice, D.Riccio, G.Ruello, "Efficient Spotlight SAR Raw Signal Simulation of Extended Scenes", *IEEE Trans. Geosc. Remote Sensing,* vol.41, pp. 2329- 2337, 2003.

[4] G. Franceschetti and R.Lanari; Synthetic Aperture Radar Processing, CRC PRESS, New York, 1999.

[5] D.P.Belcher, C.J.Baker, "High resolution processing of hybrid stripmap/spotlight mode SAR", *IEE Proc., Radar Sonar Navig*., vol.143, pp.366-374, 1996.

[6] G.Fornaro, R.Lanari, E.Sansosti, F.Serafino, S.Zoffoli, "A new algorithm for processing hybrid strip-map/spotlight mode synthetic aperture radar data", *Proc. SPIE – Int. Soc. Opt. Eng.,* vol.4173, Barcelona, Spain, pp.17-28, 2000.

[7] R.Lanari, S.Zoffoli, E.Sansosti, G.Fornaro, F.Serafino, "New approach for hybrid strip-map/spotlight SAR data focusing", *IEE Proc., Radar Sonar Navig.* vol.148, pp.363-372 , 2001.

[8] J.Mittermayer, R.T.Lord, E.Boerner, "Sliding Spotlight SAR Processing for TerraSAR-X using a new formulation of the extended chirp scaling algorithm", *Proc. IGARSS* 2003, Toulose, France, pp.1462-1464, 2003.

[9] F.Caltagirone, P.Spera, R.Vigliotti, G.Manoni, "SkyMed/COSMO mission overview", *Proc. IGARSS1998*, Seattle,USA, pp. 683-685, 1998.

[10] J.H.G.Ender, A.R.Brenner, "PAMIR – a wideband phased array SAR/MIT system", *IEE Proc., Radar Sonar Navig*., vol.150, pp.165-172, 2003.

[11] G.Franceschetti, M.Migliaccio, D.Riccio, G.Schirinzi, "SARAS: a SAR raw signal simulator", *IEEE Trans. Geosc. Remote Sensing*, vol.30, pp.110-123, 1992.

[12] G.Franceschetti, M.Migliaccio, D.Riccio, "SAR simulation of actual ground sites described in terms of sparse input data", *IEEE Trans. Geosc. Remote Sensing*, vol.32, pp.1160-1169, 1994.

[13] G.Franceschetti, A.Iodice, M.Migliaccio, D.Riccio, "A Novel Across-Track SAR Interferometry Simulator", *IEEE Trans. Geosc. Remote Sensing*, vol.36, pp.950-962, 1998.

[14] S.Cimmino, G.Franceschetti, A.Iodice, D.Riccio, G.Ruello, "Efficient Spotlight SAR Raw Signal Simulation of Extended Scenes", *IEEE Trans. Geosc. Remote Sensing,* vol.41, pp. 2329- 2337, 2003.

[15] E.Boerner, R.T.Lord, J.Mittermayer and R.Bamler, "Evaluation of TerraSAR-X Spotlight Processing Accuracy based on a New Spotlight Raw Data Simulator", *Proc. IGARSS* 2003, Toulose, France, pp.1323-1325, 2003.

[16] A. Mori, F. De Vita, "A Raw Signal Simulator for Stripmap, Spotlight and Hybrid Mode Interferometric SAR on Spaceborne Platform", *Proceedings of the SRL' Science Mission Meeting: What's next?,* Florence, Italy, 2001.

[17] G.Fornaro, "Trajectory Deviations in Airborne SAR: Analysis and Compensation", *IEEE Trans. Aerosp. Electron. Syst.*, vol.35, pp.997-1009, 1999.

Chapter 3

The problem of feature extraction from SAR images of urban areas

Extraction of features of any type from SAR images of urban scenes represents at the moment one of the most interesting subjects of research in the field of remote sensing not only for all commercial applications that can be derived but above all for the lasting and important support that it can ensure to civil protection.

That is why new and more adequate models for features extraction are studied and strongly required.

Continuous changes in urban scenarios link the problem of feature extraction to the need of "learning" from a dynamic environment. Adaptation of artificial neural networks, widely exploited in environments changing over time, allows to deal with the complex scenes represented by urban centres.

The high complexity of urban scenes and, consequently, of relative SAR images in which many typical distortion effects are emphasized, such as layover and shadow ones, often lead to face the problem of building reconstruction with a stochastic analysis of existing data. But only recently a similar approach, usually adopted with interferometric data, has been applied to a single high resolution SAR image.

In this chapter, after showing and explaining the main difficulties and advantages deriving from working with SAR images of urban areas, the most interesting approaches in feature extraction, already presented in literature, are discussed and the need of a new model-based approach is also introduced.

3.1 Man made objects in SAR images

SAR images relevant to urban centres can be very difficult to be understood and complicated to be interpreted. This is true not only for the presence of some distortion effects usually emphasized in similar frameworks (like shadow and layover) but, above all, for the increase of multiple scattering when man-made objects crowd the scene under detection [1]. In fact, contributions relative to different buildings may partially overlap

each other, so that the radar return from each building is mixed with returns from near structures.

Moreover, let us think of the high variability of urban landscape, its complex combinations of natural and man-made elements, the wide variety of materials, and objects forms and sizes.

To better understand the complexity of urban SAR images it is then useful to begin to analyze a very simple example and successively try to generalize some considerations.

To our aim let us examine the simple urban scene represented in Fig. 1.The building is modelled via a parallelepiped with flat surfaces. This implies that we do not consider the presence (and so the relative contribution to the SAR image) of windows and balconies, as well as we consider flat and not rough roofs. However, this assumption can be relaxed and a more realistic shape for modelling the building can be easily employed.

Any direction φ respect to the radar flight trajectory can be considered. We could also consider mote than one building at the same time provided that all they are isolated in a radar sense: their radar returns do not interfere with any return from other buildings in the scene.

Obviously, this is a canonical scene providing a simplified view that can fit only some particular actual scenes but it represents a preliminary compulsory step to be approached for a better interpretation of urban SAR images.

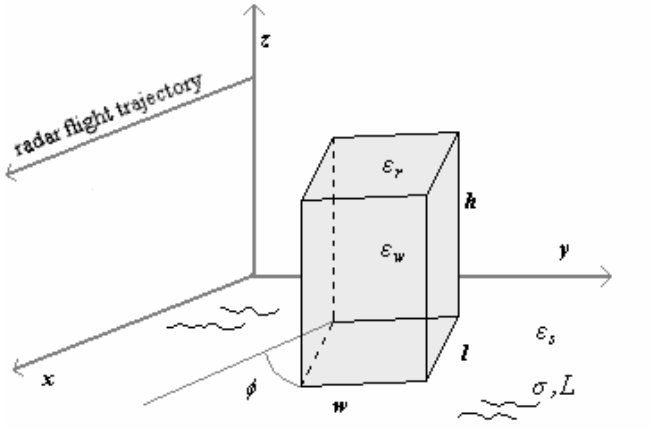

Figure 1 Geometric model of the scene.

In Fig. 1 for the model adopted all main building and ground parameters are defined: the height h, the length l and the width w of the building together with its complex dielectric constants (ε_r for the roof and ε_w for the

walls); the correlation length L and deviation standard σ of the stochastic process describing the roughness of the soil and its complex dielectric constant ε_s.

We propose to analyze the way this geometry affects the formation of SAR images once the building has been hit by the radiation.

Because of the dihedral formed by the building wall with the rough terrain, not only single scattering but also double and triple scattering contributions arise. Now, a brief but complete description of mechanisms occurring in the SAR image formation is needed. Precisely, let us illustrate how distortion effects and multiple scattering combine together in the SAR image.

Let us start with distortion effects. In literature *layover* and *shadow* are sufficiently described and it is well known why they arise: steepest profiles cause a misrepresentation of points on the image if they are visible to the sensor (layover) and a lack of signal if they are not in sight (shadow). That is why, for years, the presence of these effects on the image was considered a problem to be solved. Recently, however, it has been proved that areas affected by layover and shadow are bearer of some information when urban scenarios are investigated. For example, let us consider a canonical scene in which a wall of the building is aligned with the sensor flight trajectory: it is quite trivial, from Fig. 2, to understand that range extensions of layover and shadow are simply linked to the height of the building involved and the SAR look angle. This link still exists when the wall is not aligned with sensor flight trajectory, even if it is more complex. It is interesting to note that this is a new application of a very old idea that dates back to about 2600 years ago, when Thales of Miletus estimated the height of pyramids in Egypt by measuring the length of their shadows.

Fig. 2 also shows which “parts” of the image are affected by layover and shadow. With an intuitive but not rigorous description we could say that the layover area is the nearest in range (the coordinate of the image perpendicular to flight trajectory) while the shadow one is the farthest.

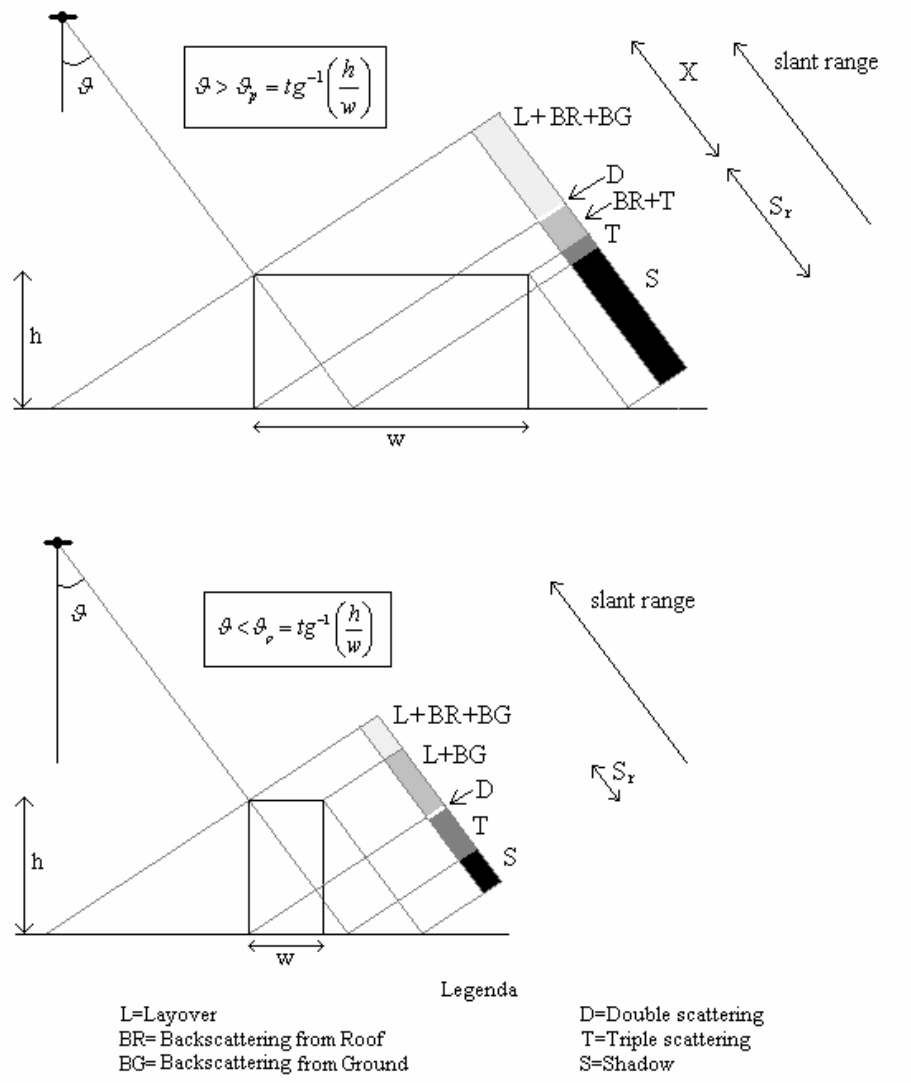

Figure 2 Side view of the scene and composition of different contributions in the SAR image.

The described distortion effects are never isolated. Multiple scattering of different orders, layover and shadow overlap always in different ways. Within this framework, first, second and third-order contributions to the radar cross section have been considered for the evaluation of backscattered

electromagnetic fields. Higher order contributions add nothing to the backscattered field to the radar antenna because the wall surface is supposed to be flat [1].

Fig. 2 and [2] detail how multiple scattering contributes to the SAR image formation of urban scenes. In this session we shall confine ourselves to point out some interactions that will be useful in the next sections:

1. In any situation, double reflection signs the passage from the end of layover and the beginning of triple scattering. So we can always say, without ambiguities, where the layover area ends.
2. The beginning of shadow, instead, is very difficult to determine because, according to circumstances, some layover can overlap. If only triple scattering adds to shadow area the problem does not hold good, being triple scattering of low intensity.
3. Single scattering from ground and roof always covers partly single scattering from wall (that is layover) thus complicating an intensity evaluation of layover area.

The description above has introduced, even if for a very simple model of urban scene, the complexity of a SAR image when man made objects are present.

We can now try to imagine how all the effects described get emphasized on real SAR images where much more buildings are present and interact among them. It surely happens, for example, that dihedral and trihedral configurations multiply, sometimes imprisoning the radar signal, or that shadow areas become so numerous that some structures are not visible for particular SAR look angles.

Many studies described in literature working with feature extraction from SAR images of urban areas reckoned with the difficulty of interpreting such a kind of “view” but nevertheless they managed to achieve very interesting results as summarized in the next paragraphs.

3.2 Information retrieval from urban SAR images: limits and benefits

The way in which simple building structures affect a real SAR image has been widely explored. Actually, the kind of man-made objects considered is so simplified that some doubts can arise about its capability of well

representing the ground truth. In fact, not only buildings are more complicated but many other structures such as streets, bridges, parking areas etc. are present in urban areas.

We understand that the respective SAR image can be of difficult analysis. Compared with optical image in which human interpretation is lead by a certain experience, the SAR image of urban areas is still today quite cryptic. This is partly due to the problematic effects described in the previous paragraph but it is also ascribable to the employment of a technology that is still young.

Even if young, SAR technology is rapidly growing up: it is sufficient to think of its latest innovations able to grant very high resolutions images. The wide band on one side and new acquisition modes on the other will soon ensure SAR sensors with excellent performance and even decimetric resolutions.

But, in spite of high resolutions, analysis and interpretation of SAR images relative to urban areas are still open questions. Difficulty in images interpretation arises for many reasons: above all, the extreme complexity and variety of urban landscape constituted by objects of different form, size and material. Moreover, for a complete description, mutability of a scenario changing over time has to be considered.

These features emphasize when resolution improves because new details become visible on the image. Consequently, we can follow, in principle, any evolution (in form or material) of a great amount of objects. In practice, in order to exploit availability of huge amount of data, we need elaboration processing and techniques being in step.

But we understand that every effort in this way is worth to be made as SAR capability of ensuring permanent monitoring, indifferent of weather conditions, is of paramount importance.

In fact, benefits that can be derived are unnumbered and SAR technology can represent an important support for civil protection. For instance, let us think of usefulness of a continuously updated information about the extension of built-up areas for a fast intervention in case of natural disaster, or of importance to monitor health conditions of roads for civil safety as well as of old town centers that need to be safeguarded.

Now, a look into the most interesting approaches that in the last years tried to retrieve a certain information from SAR images of urban areas is compulsory.

But we need first to make a preliminary statement. The most of techniques described in literature on this topic, regarding the retrieval of geometric or electromagnetic information from SAR images, usually involve

the manipulation and, consequently, the interpretation of digital images with the aid of a computer. Sometimes supported by other kind of images, (typically optical images), they try to extract information analyzing pixel value and its neighbourhoods ignoring the relationships among the radar parameters and the scene ones. It means that they are not model-based approaches unlike the deterministic method developed for this thesis and presented in the next Chapter.

3.3 Existing retrieval approaches for geometric information

Let us consider a generic urban area and let us inspect the information content of relative SAR images. A structural analysis, able to provide a macroscopic view of the scene, allows to obtain useful global information also studying SAR images with low resolution. For example, the monitoring of buildings or streets density in built-up areas, as well as the singling out of boundaries between urban and not urban areas, is possible in different ways, [3]-[5].

The dynamism of urban scenes, usually higher than those relevant to a natural landscape, justifies the use of a neural based processing. The risk of working with a strongly mutable environment, in fact, is finding processing solutions which, if strictly dependent on the problem at issue, result no more efficient in short. Instead, solutions taking into account the dynamism of the scene will be flexible and able to pursue the change taking place. Neural networks allow this kind of approach, able to adapt to the scene and its changes, thanks to its ability to learn from the environment and to modify its responses to the external stimuli even in circumstances not a priori known.

A first time of learning, the so called training phase, is requested every time we desire to update the network after that a change has taken place in the scene. But being unknown both the rapidity and the number of changes, the user will decide when an updating of the network is needed, thus defining the performance of a neural network based approach.

This kind of processing is useful when a first, even if coarse, classification of the image is desired, for example to separate vegetation from built up areas or streets [3]. Neural approach for images classification turns out to be more robust to training site selection and, above all, it is able to well recognize intrinsically heterogeneous classes [4]. But, because of possible multiple training phases, this kind of solution produces high

computational costs. In order to reduce processing times, the training phases should be reduced; however this corresponds to obtain a processing chain that is very precise on training data set but much less accurate on effective data to be tested.

In this situation, it is better to choose a different solution which, being not adapted to any training data set, shows an usually better accuracy on effective data.

A statistical approach allows to reach such a performance. Moreover, the complexity of urban scenarios, where natural and artificial objects live together, is well faced by a stochastic analysis. As a matter of fact, the urban landscape complexity presents two different aspects. The simpler one relies on the urban area elementary constituents (buildings, terrains,…) which are characterised by their different geometrical and electromagnetic parameters. The more involved source of complexity relies on the almost unpredictable ways these constituents populate the scene and interact on the radar return.

When the image resolution is improved, new details can be appreciated on the scene which shall appear much more complex. This happens when resolution is of the order of 1 meter or less. Very high resolution SAR images are notably complex and of difficult interpretation even if they are plentiful of information.

Some information from HR (High Resolution) SAR images can still be extracted with an approach based on statistical analysis [5]. In fact, we can exploit information relative to strong and low backscattering areas in which the scene can be subdivided by a simple Bayesian classification, obtained by providing training areas and considering appropriate statistics.

This way allows to work with a great variety of urban scenarios composed by structures of different forms (buildings with slope or flat roof, of rectangular or circular base etc..). But this approach, whose objective is the reconstruction of the objects in the scene, is able to supply a still structural analysis, even if more detailed.

In Table I limits and advantages of these main approaches are summarized together with some requirements and possible applications. We particularly appreciate the wide range of scenarios that can be taken into account.

Table I
Comparison among feature extraction approaches from SAR urban images.

Approach	Neural networks	Stochastic
Kind of scenario	Any	Any
Image resolution	Medium-high	High
Applications	Evaluation of building densities, boundaries between urban and non urban areas, street tracking.	Building geometric feature extraction.
Advantages	Robust to training site selection.	Able to deal with structures, in the scene, of different shapes. Good shape identification.
Limits	High computational costs.	Low accuracy of building size estimation.

But we also would like to highlight an important matter. As anticipated, these methods are good for a *macroscopic* description of a scene, it means at a level in which we make a classification of the image discriminating vegetation from built up areas and then recognizing, inside the urban area, the different kinds of structures (roads, buildings, etc.). Actually, for many kinds of applications this could be also sufficient, above all when only geometric aspects are considered. But we realize that this way of description is and will be always and only qualitative.

Another possibility to better represent the geometry of an urban areas is to improve our knowledge using more than one SAR image. Exploiting, for example, different look angles or side views it is possible to effort the lack of information in areas with shadow or layover effects.

All these methods rely on exploitation of SAR images. For sake of completeness a brief comment on use of Interferometric SAR (InSAR) in the realization of three-dimensional city models follows.

This technique exploits the coherent nature of radar signals, being the measurement based on the phase difference of two signals. It allows in theory to achieve a very fine detection being the precision of the measurement linked to the working wavelength employed. But, in practice, it does not happen, especially in areas with poor coherence where the phase information is disturbed. In these cases, the noise component has to be removed or at least reduced before further analysis. Often the noise is decreased by averaging, e.g. low-pass filtering or multi-look processing. However, this leads to reduced spatial resolution and blurred phase jumps at objects boundaries that means loosing some initial benefits.

Moreover, especially in urban areas, this technique may fail, for instance in the phase unwrapping, because radar data from urban areas are always affected by layover and shadowing effects.

This is, in a few words, the state of art for geometric feature extraction from SAR urban images.

But if our aim is attempting a *microscopic* description, if we desire a highly detailed view of reality, in which hopefully we will arrive at a complete report of an urban scene telling not only the shape of the building but its precise dimensions and constituent materials, then a completely different approach has to be taken into consideration.

In order to better understand the importance of introducing a new feature extraction rationale, the state of art is first completed with the electromagnetic parameters retrieval in the next paragraph.

3.4 State of art for electromagnetic feature extraction

Every object in a scene interacts in a singular way with the radar signal. It depends, obviously, by its shape, dimensions and roughness related to the working wavelength but also by its materials.

It is well known, for example, how important is the water content in the scene in determining the radar response. This can explain the case in which different contributions derive from similar geometries: it is sufficient to think of buildings with the same geometrical features but constituted by different materials like concrete or bricks.

The electric properties of the material of an object, influencing the degree of reflection, are described by means of the dielectric constant. If a radiant flux transfers from one medium to another, a change in the velocity of propagation occurs that depends on the wavelength used. In addition, attenuation (reduction of the energy level) by phase shifts, among other things, will be characteristic for that medium. This attenuation will be enhanced by scattering in all directions.

Both properties are usually combined into one complex number, which has computational advantages. The dielectric constant ε consists of a real part ε' and an imaginary part ε'':

$$\varepsilon=\varepsilon'-j\varepsilon'' \qquad (3.1)$$

where ε′ is the permittivity of the material and ε″ is the dielectric loss factor.

Now, understanding the way the dielectric constant of a general material affects the backscattering is a hard task and this explains, still today, how difficult is to create a model of electromagnetic backscattering. This is evidently true even for urban areas where the different materials involved are a lot.

Then, in this thesis, for electromagnetic feature extraction we mean the possibility of retrieving the complex dielectric constant of an urban surface (a building roof or wall, the street pavement etc.). For the definition given in Eq. (3.1) it means to define two unknowns.

But from literature we realize that, especially for urban areas, this is still an open issue.

Some empirical models have been developed for radar backscatter of soils, crops, forest vegetation etc., but for urban geometries they are still inadequate. We have only a complete electromagnetic backscattering model for a canonical structure [1,2] that will be described and employed in the next chapter.

This lack of models explains why, till today, only a classification of urban areas has been possible by means of SAR images. In fact, without models nobody is able to extract such an information because there are not equations to be inverted.

And we know that this is the real challenge. The impact that a similar retrieval of information would have on applications is of utmost importance. Let us think of the possibility of checking the presence of water infiltration in building walls or of amianthus, widely employed in the past in building industry as insulating material but now forbidden by the law in many countries for its demonstrated carcinogenic properties.

Being aware of the complexness of our aim as well as of its need we will try, in the next chapters, to lay the foundations for a similar study.

References

[1] G.Franceschetti, A.Iodice, D.Riccio, “A canonical problem in electromagnetic backscattering from buildings”, *IEEE Trans. Geosc. Remote Sensing*, vol.40, pp.1787-1801, 2002.

[2] G.Franceschetti, A.Iodice, D.Riccio, G.Ruello “SAR raw signal simulation for urban structures”, *IEEE Trans. Geosc. Remote Sensing*, vol.41, pp.1986-1995, 2003.

[3] F.Dell'Acqua, P.Gamba, "Detection of urban structures in SAR images by robust fuzzy clustering algorithms: the examples of street tracking", *IEEE Trans. Geosc. Remote Sensing*, vol.39, pp.2287-2297, 2001.

[4] T.Macrì Pellizzeri, P.Gamba, P.Lombardo, F.Dell'Acqua, "Multitemporal/Multiband SAR Classification of Urban Areas Using Spatial Analysis: Statistical Versus Neural Kerned-Based Approach", *IEEE Trans. Geosc. Remote Sensing*, vol.41, pp.2338-2353, 2003.

[5] M.Quartulli, M.Datcu, "Stochastic Geometrical Modeling for Built-Up Area Understanding from a Single SAR Intensity Image with Meter Resolution", *IEEE Trans. Geosc. Remote Sensing*, vol.42, pp.1996-2003, 2004.

Chapter 4

The deterministic approach of feature extraction

In the previous Chapter, the state of art of feature extraction from SAR images has been discussed. In the most cases, in the mentioned works, a stochastic analysis is a compulsory step to face the problem of high complexity in SAR images of urban scenes.

However, an alternative deterministic approach, able to invert geometric and electromagnetic models, is still strongly required and needed. Till few years ago, it was a hard and difficult task due to the lack of physical and mathematical models able to describe the complex interactions among the radar signal and the man made objects in the scene. In [1]-[2], a first attempt in this direction was made: first, a direct backscattering model for a single element of an urban scene was presented in [1]; this backscattering model was then included in a SAR raw signal simulator for urban structures [2]. Availability of such a simulation tool is a fundamental support in developing the idea of a deterministic extraction of geometric and electromagnetic parameters from HR SAR images [3]. The backscattering model and the SAR simulator provide a full (analytical and numerical) set of direct relationships between the parameters of each building of the urban area and some measurable parameters in the corresponding SAR images: all this material provides the background for the inverse problem that we propose to solve via deterministic approach.

The basic idea presented in general in [2] is now developed in details, discussed and completed by many examples.

In the next paragraphs, we define a set of geometric and radiometric parameters measurable on a SAR image of isolated buildings (i.e., sizes of layover and shadow areas, orientation angle of the building, radar cross section), and a set of geometric and electromagnetic parameters to be estimated (i.e., height, length and width of the building; complex dielectric constants of walls, roof and soil; soil roughness parameters).

Then, we look for a set of analytical expressions that link parameters to be estimated to the measured ones. The obtained relationships allow us to write, for each geometric and electromagnetic feature of an isolated building, a set of independent equations whose solution supplies multiple determinations of the same parameter. A general retrieval scheme is proposed and is described in detail in the case of estimation of the building

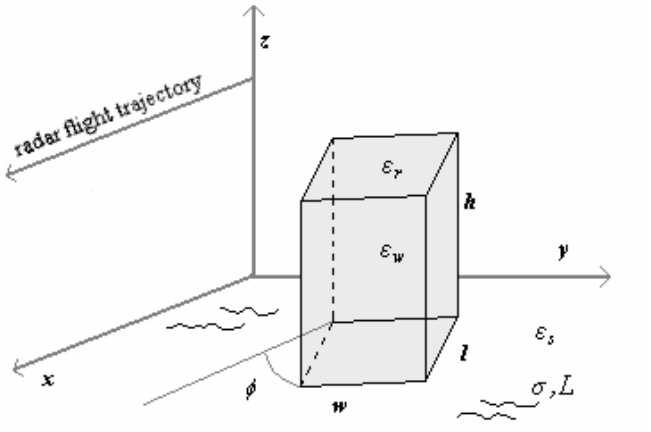

Figure 1 Geometric model of the scene.

height. Some examples of building height retrieval from simulated SAR images (for which the "ground truth" is perfectly known) are presented in order to assess the accuracy of the retrieval scheme. Finally, a sensitiveness analysis is proposed to study the robustness of the proposed approach.

4.1 Geometric and electromagnetic models

Let us choose to represent a building with the same geometrical model introduced in Chapter 3. For sake of simplicity, that model is reported again in Figure 1.

We also remind the assumptions needed for the solution scheme that will be presented in the next. The building is modelled via a parallelepiped with flat surfaces, the roof is flat and not rough. It is based on a rough terrain and other buildings can be considered in the scene provided that there are mot mutual interactions among them.

Now, we can define a finite set of *geometric* parameters to be estimated for the building and the surrounding soil:

- Building height *h*;
- Building length *l*;
- Building width *w*;

- Roughness parameters, i.e., the deviation standard σ and the correlation length L of the Gaussian stochastic process describing the soil surface profile.

In the same way, let us define a set of *electromagnetic* parameters to be estimated for the building and the surrounding soil:

- The complex dielectric constant of walls ε_w;
- The complex dielectric constant of the roof ε_r;
- The complex dielectric constant of the soil ε_s.

The above list of parameters represents the geometric and electromagnetic information that we propose to extract from a single high resolution SAR image. These cannot be directly measured on a SAR images of the building. So we need to define also a set of geometric and electromagnetic parameters that are directly measurable on SAR images.

Now, in Chapter 3 a brief but complete description of mechanisms occurring in the SAR image formation has been presented. It implicitly referred to some parameters measurable on a SAR image: layover and shadow range sizes and the radar cross section σ^o. The angle between the wall of the building and the sensor trajectory flight φ is measurable too. Obviously, these parameters are strictly linked to those defined and listed above. Precisely, a set of analytical expressions relating parameters to be estimated to the measured ones can be found as synthesized in Fig. 2 and it is what we do in the next.

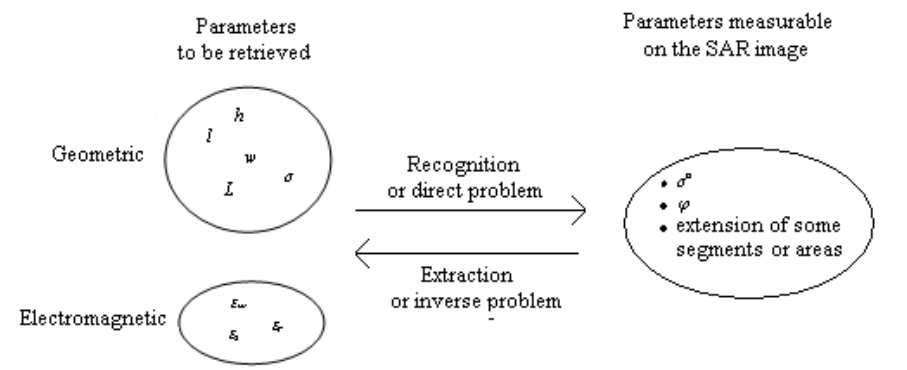

Figure 2 Statement of the problem: from the parameters measurable on the SAR image to those to be retrieved.

But we first need of a sound electromagnetic model, able to sufficiently describe the radar return from a canonical structure represented by a building on a rough terrain. Such a model is necessary if we want to extract detailed information from a SAR image.

Now, numerical methods are available but, unlike analytical ones, they do not show the functional dependence between the scattered electromagnetic field and the scene parameters which represents a basic previous statement in our work. In addition, analytical approaches can considerably reduce computational loads when efficient closed-form solutions are available. And this is our case, being the analysis presented in this work based on geometrical optics (GO) and zero-order physical optics (PO) solutions to the scattering problem, which are shown to lead, when applicable, to evaluations in closed form for each contribution to the scattered field [1].

In [1] these closed forms have been found and represent in [2] the foundations of a SAR raw signal simulator of wide applicability relative to urban structures. Starting from [2], functional dependence among geometric and electromagnetic parameters can be highlighted, whereas the simulator of [2] can be used to test the retrieval algorithms under development.

4.2 Inversion procedure

As regards geometric parameters, the connexions that can be derived are listed in Table I.

Table II, instead, shows which scattering contributions are influenced by electromagnetic parameters.

The lists in Tables lead, for each of geometric and electromagnetic parameters, to a system of equations whose solution provides multiple and independent determinations of the same quantity. This is of paramount importance and utility for many reasons. In fact, availability of more than one determination of the same parameter, each one obtained in a different and independent way (i.e., with independent error sources), allows us to improve the evaluation of every parameter in a least square framework (as explained in § 4.3.1).

Table I

Relationships among geometrical parameters and those measurable on the SAR image.

The building height h is linked to	The building length l is linked to	The building depth w is linked to	The angle φ is linked to	The roughness parameters σ and L are linked to
- layover range size - shadow range size - radar cross section through ▪ single scattering from wall ▪ double scattering ▪ triple scattering	- the shape of the building in the SAR image (particularly the azimuth extension of building image when ψ=0) - radar cross section through ▪ single scattering from wall ▪ double scattering ▪ triple scattering	- the shape of the building in the SAR image (particularly, the range extension of single scattering from roof when ψ=0)	- the shape of building image - radar cross section through ▪ single scattering from wall ▪ double scattering ▪ triple scattering	- radar cross section through ▪ single scattering from ground ▪ double scattering ▪ triple scattering.

Table II

Relationships among electromagnetic parameters and those measurable on the SAR image.

The complex dielectric constant of building wall ε_w is linked to	The complex dielectric constant of building roof ε_r is linked to	The complex dielectric constant of building wall ε_w is linked to
- radar cross section through ▪ single scattering from wall ▪ double scattering ▪ triple scattering;	- radar cross section through ▪ single scattering from roof	- radar cross section through ▪ double scattering ▪ triple scattering.

Let us now move to the second phase called "phase of extraction".

We here focus our attention on geometrical parameters, but a similar procedure can be adopted for electromagnetic feature extraction. Precisely, let us imagine that we want to extract information on the height h, the length l and the width w of an isolated building from a HR SAR image. In order to do that, we use relationships among (h, l, w) and measurable parameters on the SAR image. As previously highlighted, these analytical expressions are all in closed form and descend from the geometric and the electromagnetic models adopted, respectively, for the description of the scene and the computation of signal backscattered to the radar. Let us explicitly write each parameter to retrieve as a function of the other, assumed known. We first consider the building height h.

From Table I we find that h determines size of layover L_r, shadow S_r areas and influences radar cross section σ^o through single scattering from wall, double and triple scattering. A solution scheme for height extraction is now derived.

From layover and shadow sizes we get information on h in the following way [9]:

- if $\vartheta > \vartheta_p = tg^{-1}\left(\frac{h}{w}\right)$

  - $h = \frac{L_r}{\cos\vartheta}$ (4.1)
  - $h = S_r \cos\vartheta$ (4.2)

- if $\vartheta < \vartheta_p = tg^{-1}\left(\frac{h}{w}\right)$, layover partly masks shadow, and h can be extracted only from L_r:

  - $h = \frac{L_r}{\cos\vartheta}$

where ϑ is the look angle of the sensor.

From multiple scattering, converting relative equations presented in [1] from implicit to explicit form we get the analytical expressions linking h to geometric and radiometric parameters.

As regards double scattering contributions, we distinguish two cases according to the roughness parameters and, consequently, to the approximation adopted in the Kirkhhoff approach [1]. In fact, we use GO to evaluate the field reflected by the wall toward the ground (first bounce) or the sensor (second bounce) and GO or PO (according to the ground surface

roughness) to estimate the field scattered by the ground toward the wall (first bounce) or the sensor (second bounce).

For triple scattering only wall-ground-wall contribution is considered. Adopting GO solution for wall scattering, this contribution is evaluated either with GO-GO-GO or GO-PO-GO method according to the ground surface roughness.

All these contributions are linked to the building height as mentioned above and shown below:

- From GO-PO solution for double scattering

$$h = \frac{\sigma_{A0}^2 \cdot \exp\left[\dfrac{\left(2kL\,\mathrm{sen}\varphi\,\mathrm{sen}\,\vartheta\right)^2}{4m}\right]}{l\tan\vartheta\cos\varphi\exp\left(-4k^2\sigma^2\cos^2\vartheta\right)\displaystyle\sum_{m=1}^{\infty}\frac{\left(2k\sigma\cos\vartheta\right)^{2m}}{m!}\pi\frac{L^2}{m}} \tag{4.3}$$

where

- $k=2\pi/\lambda$ is the wavenumber
- $\sigma_{A0}^2 = \left\langle \left| I_{A0}{}^2 \right| \right\rangle - \left| \left\langle I_{A0} \right\rangle \right|^2$ with I_{A0} standing for the surface integral evaluated over the ground portion hit by wall surface [1];

- From GO-GO solution for double scattering

$$h = \left|\sigma^\circ\right| \frac{8\pi^2\cos^2\vartheta\cdot\sigma^2\left(2/L^2\right)\cdot\exp\left[\dfrac{\tan^2\vartheta\sin^2\varphi}{2\sigma^2\left(2/L^2\right)}\right]}{\left|S_{pq}\right|^2 l\tan\vartheta\cos\varphi\left(1+\tan^2\vartheta\sin^2\varphi\right)} \tag{4.4}$$

where S_{pq} is the generic element of scattering matrix, with p and q each standing for h or v (horizontal or vertical polarization);

- From GO-PO-GO solution for triple scattering

$$h = \frac{\sigma_{A_0}^2 \cdot \exp\left[\dfrac{\left(2kL\,\mathrm{sen}\,\vartheta\right)^2}{4m}\right]}{l\tan\vartheta\cos\varphi\exp\left(-4k^2\sigma^2\cos^2\vartheta\right)\displaystyle\sum_{m=1}^{\infty}\frac{\left(2k\sigma\cos\vartheta\right)^{2m}}{m!}\pi\frac{L^2}{m}} \tag{4.5}$$

- From GO-GO-GO solution for triple scattering

$$h = \left|\sigma^{\circ}\right| \frac{8\pi^2 \cos^4 \vartheta \sigma^2 \left(2/L^2\right) \cdot \exp\left[\dfrac{\tan^2 \vartheta}{2\sigma^2 \left(2/L^2\right)}\right]}{\left|S_{pq}\right|^2 l \tan \vartheta \cos \varphi} \tag{4.6}$$

where A_0 stands for the portion of the ground hit by radiation reflected by the wall.

Similar results are obtained when we try to retrieve information on the building length l from radar cross section: it is sufficient to exchange l and h in Eqs. (4.3-6) to obtain equations from which l can be retrieved. As regards building length l and width w extraction from geometric parameters on SAR image a different discussion is required.

For a generic direction $\varphi \neq 0$, l can be extracted from geometric parameters measuring, on the azimuth-slant range SAR image, the distances dx and dr, indicated in Fig. 4 and linked to l through the expressions:

$$dy = \frac{dr}{\sin \vartheta} \tag{4.7}$$

$$l = \sqrt{dx^2 + dy^2} \ . \tag{4.8}$$

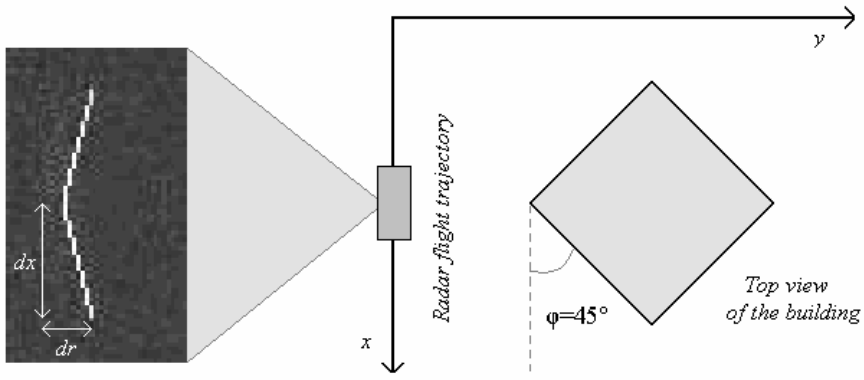

Figure 4 Top view of the urban scene and relative SAR image.

Actually, for the symmetry of the problem which produces parallel boundaries among different contributions, we can have multiple determinations of *dx* and *dr* too. In Fig. 5 this is shown very well by means of a detailed description of how different contributions overlap for the scene represented in Fig. 4. According to the situation at issue, we can carry on one or all of these measures on the image.

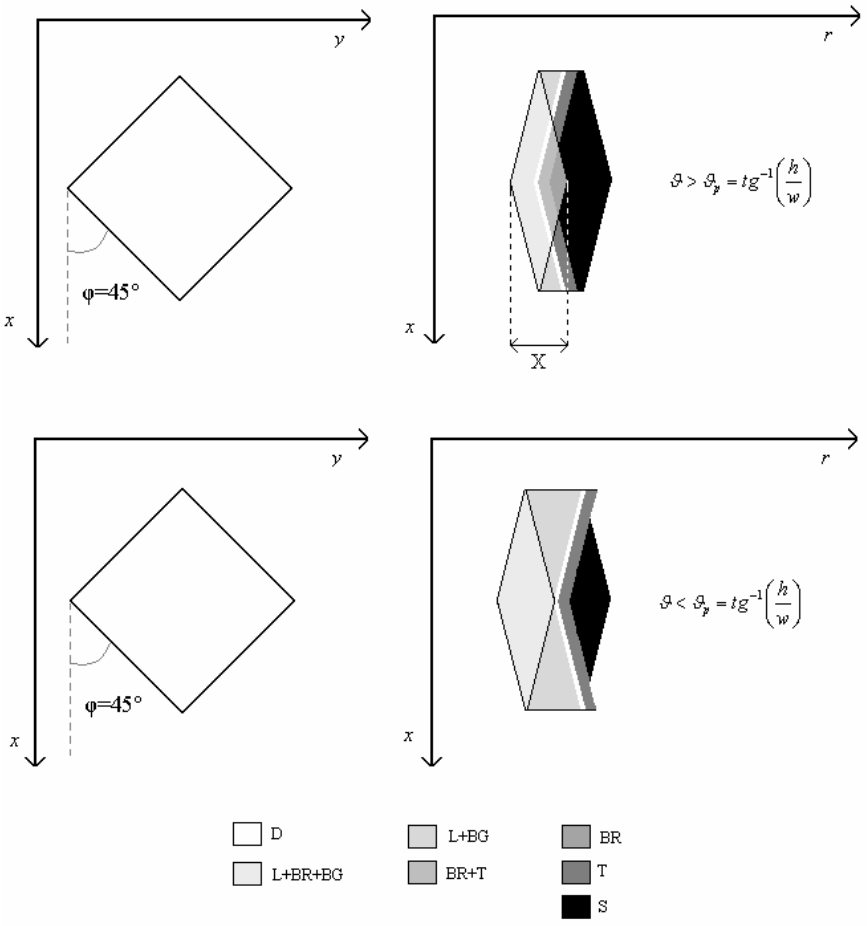

Figure 5 Composition of different contributions in the SAR image for a building oriented with a 45° angle with respect to the radar flight trajectory. Top: $\theta > \theta_p$. Bottom: $\theta < \theta_p$.

For the extraction of building width w, analogous considerations can be done for a generic direction φ. In a different way, as shown in [4], w can be extracted by measuring, depending on the situations, either the range extension X or S_r (see Fig. 2 in Chapter 3):

- if $\vartheta > \vartheta_p = tg^{-1}\left(\frac{h}{w}\right)$

  ▪ $$w = \frac{X}{\operatorname{sen}\vartheta}\cos\varphi \tag{4.9}$$

- if $\vartheta < \vartheta_p = tg^{-1}\left(\frac{h}{w}\right)$ and h has been already extracted

  ▪ $$w = \left[\frac{S_r}{\operatorname{sen}\vartheta} - h\tan\vartheta\right]\cos\varphi \tag{4.10}$$

Obviously, the roles of l and w are interchangeable and so the previous distiction about the information extraction for these parameters is not strictly necessary.

Now, for each of the geometrical and electromagnetic parameters defined in the previous section similar solution schemes can be derived thus obtaining a full and complete framework for deterministic extraction of building parameters.

4.3 Extraction examples on simulated SAR images

4.3.1 Retrieval procedure

Considerations reported in the previous paragraphs lead to define the following general retrieval procedure: given a set of parameters to be retrieved,

STEP 1: Measure some relevant parameters on the SAR image (layover and shadow sizes, radar cross section).

STEP 2: Use analytical links of § 4.2 to write a system of equations whose unknowns are the parameters to be retrieved.

STEP 3: Solve the system of equations in the least square sense.

Obviously, this general procedure needs to be better specified for each parameter or set of parameters to be retrieved. In the following we will focus our attention on the retrieval of the building height.

It is clear that STEP 1 is implicitly based on the capability of distinguish some particular regions on the SAR image. For example, building height evaluation from layover and shadow, or from double scattering intensity, strongly depends on ability in picking up and extracting these regions on the image thus separating them from the context around.

This aim has rarely a trivial solution, nor a general method to adopt, especially when actual SAR images are considered, being strictly dependent on the scene at issue. Some fundamentals of picture segmentation are then needed to face every time the problem with the best instrument [5].

In the following, our effort will be dividing the picture, i.e. the SAR image, into different parts having some meaning for us according to the discussion of previous paragraphs.

Indeed, it is simple to realize that our goal of detect regions can be seen as a problem of region *boundaries* identification. In fact, thanks to a-priori knowledge of some mechanisms occurring in SAR image formation, we need only to distinguish in the picture the edges of the regions of interest because some experience can tell us which contribution the edges contain.

In this framework we do not face the problem of an unsupervised segmentation, being our task the check of feasibility of deterministic building height retrieval. So, in the following, supervised region/edge detection will be considered.

Once the layover, shadow and double reflection areas have been identified, we have to measure the sizes of layover and shadow and the radar cross section of the double reflection area.

Measuring layover and shadow sizes, and also the wall orientation angle φ, are operations whose accuracy depends on the *geometric* resolution of the SAR image, but they are conceptually very simple. Conversely, measurement of the radar cross section requires the use of radiometrically calibrated SAR images. If this is not the case, a multiplicative unknown constant, due to unknown attenuation, and an additive unknown constant, due to the background noise, must be added to the radar cross section in Eq. (4.4). These two unknown constants can be computed from Eq. (4.4) itself if the heights of at least two buildings in the scene are known. The computation of these unknown constants will be referred to as “calibration operation” in the following.

With regard to STEP 2, we realize, for the case at issue, that not all the equations linking the height to the parameters to measure on the SAR image are suitable. For example, triple scattering, even if contemplated in the

modelling, is disregarded for the height estimation, being usually of negligible intensity. In the case at hand, three equations in the single unknown h can be written: Eqs. (4.1), (4.2) and (4.3) or (4.4), according to the expected soil roughness.

Finally, in STEP 3, these equations are solved in the least square sense, i.e., multiple determinations of the height are considered together in order to supply the most precise evaluation of the height. This can be done by defining an appropriate cost function (the integral square error) to minimize with respect to h:

$$E = \sum_{i=1}^{N} a_i \left(h - h_i \right)^2 \tag{4.11}$$

where N is the number of multiple determinations of the same parameter h (in the considered case, N=3), h_i is the i-th determination of h, a_i is the appropriate weight for the i-th error function h_i-h. Actually, this way requires an experience able to determine the values of the weights a_i, which means that we should be confident with the accuracy of each procedure of extraction. But being our aim that of suggesting a general method we limit to some considerations for the case at issue, leaving to future work the task of deepening the most interesting cases.

Accuracy of the determination of h from Eqs.(4.1,2), i.e., from geometric parameters (layover and shadow range extensions), depends of course on the accuracy of measurements of these parameters, which in turns depends on geometric resolution, as already underlined. In addition, the effect on h accuracy of a given error on the layover size increases with the incidence angle, whereas the effect on h accuracy of a given error on the shadow size decreases with the incidence angle, so that the relative weights of determinations of h based on Eqs. (4.1) and (4.2) depend on the incidence angle.

The evaluation of a weight for the error committed in the building height retrieval from double reflection is much more complicated. In fact, accuracy of height retrieval in this case depends on the accuracy of the measurement of the radar cross section and of the wall orientation angle, and also on the accuracy of knowledge of soil roughness parameters and of wall and soil dielectric constants. Accuracy of the measurement of the radar cross section depends on radiometric resolution, and also on the size of the double reflection area: the larger the area, the larger the number of pixel whose intensity can be averaged to reduce the speckle noise. With regard to the measurement of the orientation angle, its accuracy depends on the geometric resolution. However, some preliminary results on simulated images [6]

seems to indicate that the effect of inaccuracy of the orientation angle on the height estimation are moderate. A complete analysis of this issue is currently being performed. Finally, let us consider the effects of inaccuracy of knowledge of soil roughness and of soil and wall dielectric properties. Actually, inaccurate knowledge of these parameters may seriously affect the final height accuracy. However, if these parameters are approximately uniform all over the scene, the effects of such inaccurate knowledge almost completely cancel out in the calibration operation defined above. In fact, such errors can be, in first approximation, included in the unknown multiplicative constant.

In practice, guidelines to the choice of proper weights can be provided by results of application of the retrieval procedure to simulated SAR images, shown in the following.

4.3.2 Retrieval results

In order to test the procedure described in the previous section, we apply it to simulated SAR images.

SAR raw signals of different cases of isolated buildings on rough terrain have been simulated and processed, letting geometrical and electromagnetic parameters vary as well as the building orientation with respect to the sensor flight trajectory.

In Table III, geometrical and electromagnetic parameters regarding the scene described in Fig. 6 are reported. Fig. 7, instead, represents the simulated SAR image of the scene represented in Fig. 6.

Table III

Geometric and electromagnetic parameters describing the scene considered in the simulation examples.

Top building dimensions (length x width x height)	100 m x 100 m x 45 m
Central building dimensions (length x width x height)	100 m x 100 m x 40 m
Bottom building dimensions (length x width x height)	100 m x 100 m x35 m
Roof and wall dielectric constant	3
Roof and wall conductivity	0.01 S/m
Ground dielectric constant	4
Ground conductivity	0.001 S/m
Ground standard deviation	0.19 m
Ground correlation length	1.54 m
Image resolution (slant range x azimuth)	4.839 m x 2.571 m

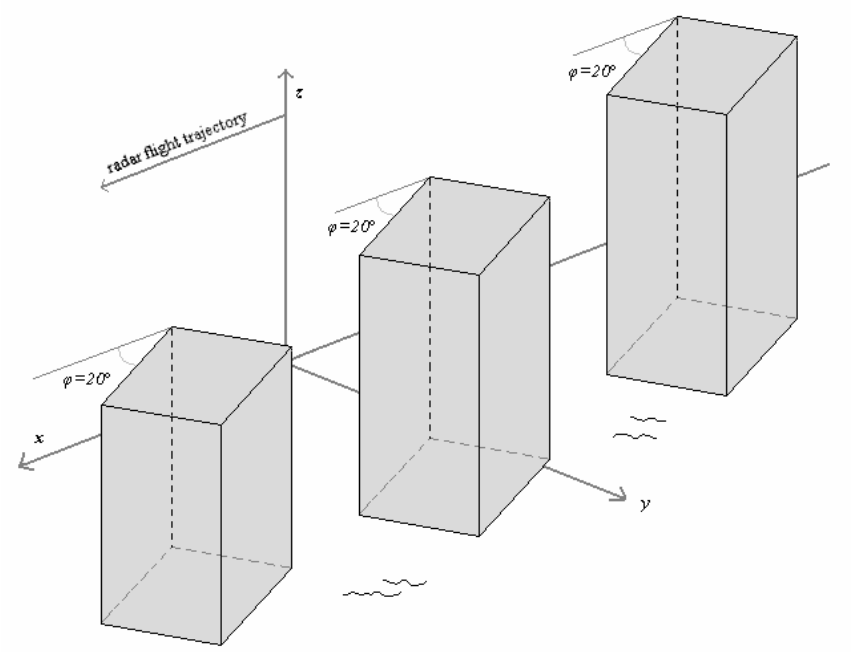

Figure 6 3-D view of a canonical scene with building wall orientation of 20 degrees.

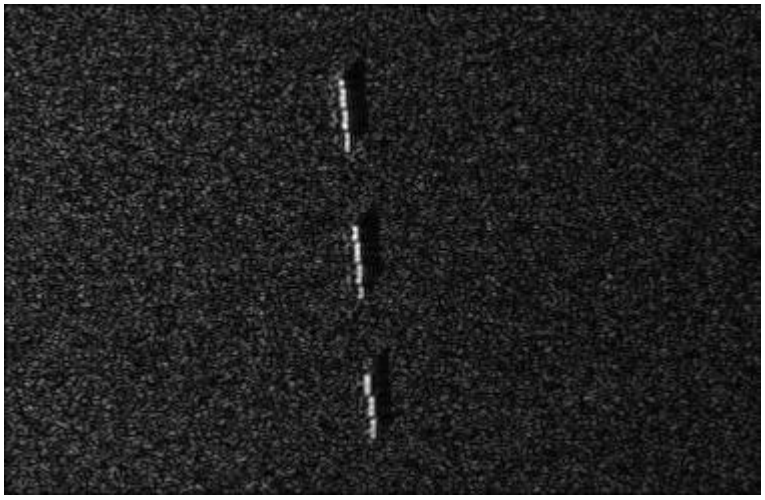

Figure 7 Simulated SAR image of the scene represented in Fig. 6.

Length and width dimensions are not typical of buildings in urban centres but they have been chosen so large in order to compare the height extraction from radiometric parameters with that one from shadow and layover.

For the sake of simplicity we supposed the buildings having the same dielectric constants, but a different electromagnetic behaviour can be considered for each of them.

For this simulation example, horizontal polarization has been considered both in transmitting and receiving mode. Radar parameters adopted are relative to a hypothetic, but not really existing, airborne sensor functioning in L-band with a look angle of 30 degrees.

Now, let us suppose that, for roughness parameters involved, Geometric Optics (GO) can represent a reasonable approximation for both bounces of double scattering. This is the case, for example, of a building with a garden in front, whatever is the working frequency in the microwave range. But if the building is placed on a bare soil, it will appear rough in the Ka band and smooth in the L one [7]; that is why the same approach with different approximations has to be adopted according to the surface roughness.

As we can see from Fig. 6 and Table III, in this first example the same electromagnetic features and the same orientation of 20 degrees with respect to the radar flight trajectory have been considered for the three buildings in the scene, but they have different heights.

In all simulations the presence of at least three buildings is considered, and we assume that we know the height of two of them in order to perform the calibration operation described in § 4.3.1. In any case, if not a-priori known, the heights of the two calibrator buildings can be determined by means of the geometric approach.

Now, for the scene at hand, let us assume that the calibrators are the buildings in the top and in the bottom of the SAR image. So, we want to retrieve information on the central building height. It is simple to verify that, being $\theta > \theta_p$ for the higher building in the top, this relation is also verified for the other buildings and, in particular, for the central one. So, both Eqs. (4.1), (4.2) can be applied for the height retrieval.

This task has been carried on by means of a range cut of the building contribution. All the values of the electromagnetic field contained in the cut have been plotted. From these plots, pixels belonging to layover or shadow area have been counted and Eqs. (4.1), (4.2) have been applied. For this first example, results for building height are listed in Table IV. The relative errors are also listed and evaluated as the difference between the retrieved height h_e and the true one h.

Table IV
Retrieval results for the scene simulated in Fig. 7.

Central building height estimations and errors	**Example n.1**	
	Height h [m]	Error $e=h_e-h$ [m]
from shadow	42.73	2.73
from layover	32.89	-7.11
from double reflection	38.60	-1.40

Now, let us move to the building height extraction from the double reflection. For this method, the first step is to isolate, for each building, the double reflection contribution. As we already said, this delicate procedure can be carried on by some software for image post processing optimized for this purpose. After having collected all pixels interested by this contribution, the relevant grey levels are averaged and this mean value is directly proportional to the radar cross section (after the calibration operation) which is linked to the building height by Eq. (4.4).

This "cut and collect" operation is repeated for the calibrators in order to get the calibration constants and then for all the buildings in the scene whose heights need to be retrieved.

In Table IV the building height value retrieved by the double reflection contribution is also listed. This result is really interesting because it shows that building extraction from radiometric parameters can be much better than that one from geometric parameters (at least for the considered scene and SAR system resolution). This means that in Eq. (4.1) a higher weight can be assigned to term relative to height retrieval from double reflection radar cross section.

Now, let us consider a slightly different scene. This time, as shown in Fig. 8, the buildings present different orientations with respect to the radar flight trajectory which are: from top to bottom, 30, 0 and 45 degrees. The heights and the other parameters in the scene are left unchanged with respect to the Example n.1. The relative simulated SAR image is reported in Fig. 9.

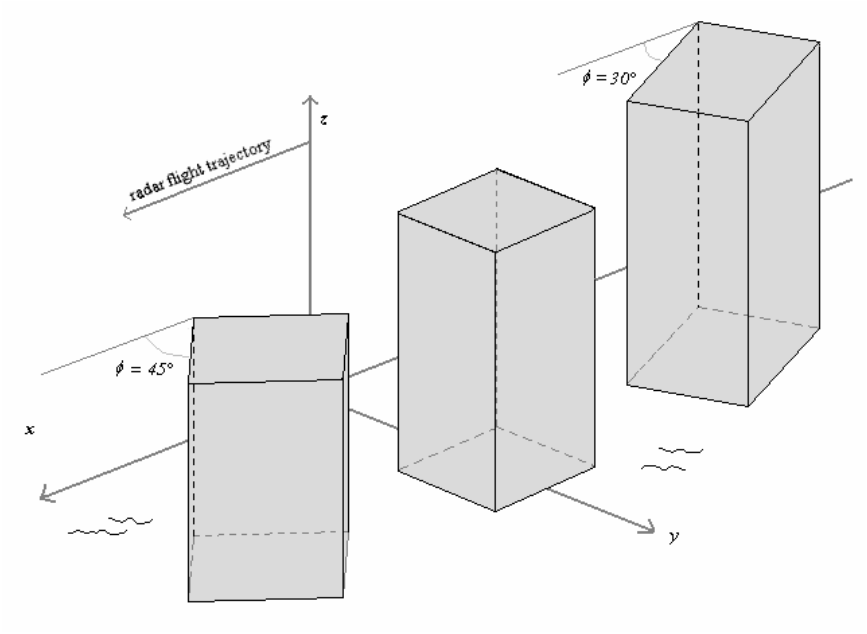

Figure 8 3-D view of a canonical scene where building wall orientation is, from the top to bottom, 30, 0 and 45 degrees.

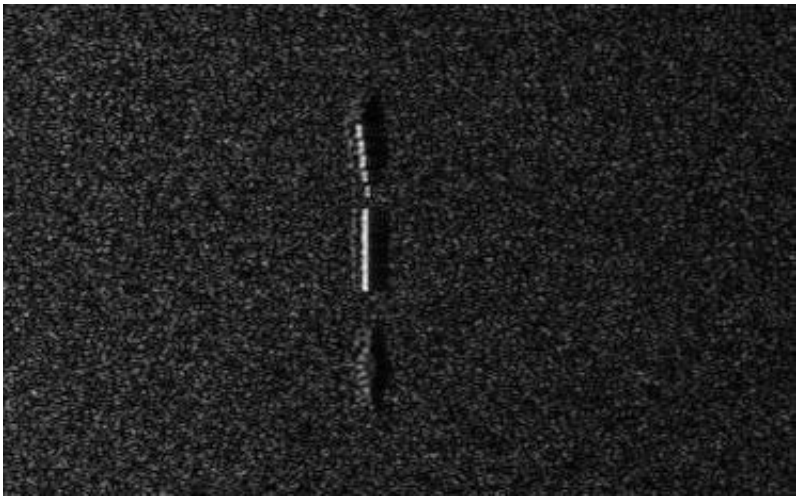

Figure 9 Simulated SAR image of the scene represented in Fig. 8.

Table V
Retrieval results for the scene simulated in Fig. 9.

Central building height estimations and errors	**Example n.2**	
	Height h [m]	Error $e=h_e-h$ [m]
from shadow	42.73	2.73
from layover	32.89	-7.11
from double reflection	38.63	-1.37

Even if this situation is still canonical, considering different orientations is surely more realistic and consents to better understand the potential of an application of this feature extraction approach to real SAR images where, obviously, the buildings are not always aligned. Also now the results are interesting, see Table V. As we could expect, we have exactly the same results as in Example n.1 for the building height retrieved from layover and shadow (in fact, the geometric resolution is the same in the two examples). For the extraction from double reflection the result is different, even if very similar, because according to Eq. (4.4) a change in φ, left unchanged the height, produces a change in the double reflection contribution to the radar cross section and, consequently, a different distribution of the grey levels in the SAR image. Nevertheless, the result is still really promising.

A huge amount of other simulations of SAR images, relative to urban scenes with very different geometries, have been carried out and every time promising results assessing the feasibility of the method have been obtained.

4.4 Sensitiveness analysis and error propagation

In previous paragraphs, we showed that, at least in theory, the building height can be retrieved not only from geometric parameters but also from radiometric ones measurable on SAR images.

But there the good and promising results in building height retrieval are paid with a high a-priori knowledge of some parameters characterizing the scene, necessary for the application of deterministic method. So, the influence of such knowledge on final results needs to be investigated.

Now, we propose to look into the applicability of deterministic extraction to actual SAR images, studying the influence of some

(inaccurately known) parameters on those to be retrieved. Precisely, the analysis has been performed on scene and radar parameters influencing the building height retrieval from the double reflection contribution to the radar cross section.

There are principally two ways in which a sensitiveness analysis can be lead. The first one is the analytical way by means of which a quantitative and general expression, relating the error on the knowledge of ground truth to the one on height valuation, can be found. Sometimes, such an analytical expression cannot be obtained, or it is too involved to be used in practice. In this case, an empirical sensitiveness analysis based on simulation examples can be more convenient, even if it does not lead to very general conclusions.

For the building height retrieval by deterministic method, both quantitative and qualitative analyses have been carried out for a valuation of error propagation and are illustrated in the following.

4.4.1 Theoretical analysis

In a more synthetic and symbolic way, expressing S_{pq} in terms of ε_s and ε_w that are the complex dielectric constants of the soil and the building wall, respectively, Eq. (4.4) can be summarized as

$$h = f\left(\sigma^o, \vartheta, \varphi, l, \sigma, L, \varepsilon_s, \varepsilon_w\right) \tag{4.12}$$

Now, some of the scene parameters in Eq. (4.4), even if a-priori unknown, can be extracted in a few steps from the SAR image. For this reason, here we shall refer to them as to "partially unknown" parameters. The radar cross section σ^O and the angle φ belong to this set: in fact, the first one is known, except for a calibration constant, by measuring the grey levels of the double reflection contribution in the SAR image, while the second one can be readily retrieved by estimating the orientation of some bright lines on SAR images and only knowing the radar parameters.

Instead, we termed as "totally unknown" those parameters that can not be readily retrieved, including, for instance, all the parameters of the stochastic process employed to describe the soil roughness, and the complex dielectric constants of objects of different material in the scene. The introduced terminology is linked to the complexity (in terms of number of needed SAR images, kind of image, number of steps, linearity or not linearity in extraction procedure) of the existing techniques to estimate them from the SAR images. Moreover, for many reasons, ground truth on these parameters can be often not available because of rapid changes in the scene or not

accessibility of the scene itself. So, an investigation of the influence of an imperfect knowledge of some parameters on the building height retrieval, by means of deterministic method, is needed and follows.

Let us consider, for example, an imperfect knowledge of "totally unknown" parameters, in particular of soil roughness parameters σ and L. For the sake of simplicity, we consider one error at a time. Then, if we know the standard deviation σ with an error $\Delta\sigma$, it means that the building height is known with the following error:

$$\Delta h = \frac{\partial f}{\partial \sigma}\Delta\sigma \tag{4.13}$$

with

$$\frac{\partial f}{\partial \sigma} = h\left[\frac{2}{\sigma} + \frac{\tan^2\vartheta\sin^2\varphi}{\left(2/L^2\right)}\left(-\frac{1}{\sigma^3}\right)\right]. \tag{4.14}$$

We can note that, for a building wall parallel to the radar flight trajectory, i.e. for φ=0, the error will be:

$$\Delta h = 2h\frac{\Delta\sigma}{\sigma}. \tag{4.15}$$

Equations (4.13-15) state the higher the building the bigger the error on height evaluation due to an error on ground roughness knowledge. Moreover, being $0<\theta<\pi/2$ and $0<\varphi<\pi/2$, the error Δh presents the same signum of $\Delta\sigma$. Finally, for φ=0, the height relative error is twice the relative error on σ.

Analogously, a simple quantitative analysis can be done considering an error on the correlation length L leading to:

$$\frac{\partial f}{\partial L} = h\left[-\frac{2}{L} + \frac{\tan^2\vartheta\sin^2\varphi}{2\sigma^2}\left(L\right)\right] \tag{4.16}$$

$$\Delta h = -2h\frac{\Delta L}{L} \tag{4.17}$$

Very complex derivatives, instead, need to be computed when we try to evaluate the consequences resulting from an error on the knowledge of the angles φ or θ. In fact, from Eq. (4.4) we see that the relationship between h

and φ or θ is really intricate, also because of the scattering element S_{pq} which is different for every couple of transmitting/receiving polarization modes.

In the case of the angle φ, an imperfect knowledge of this parameter would influence the height retrieval according to the weight

$$\frac{\partial f}{\partial \varphi} = h \cdot \left\{ -2 \frac{1}{\left|S_{pq}\right|} \cdot \frac{\partial \left|S_{pq}\right|}{\partial \varphi} + \tan \vartheta - \frac{\operatorname{sen} 2\varphi \tan^2 \vartheta}{1 + \tan^2 \vartheta \operatorname{sen}^2 \varphi} + \operatorname{sen} 2\varphi \right\} \tag{4.18}$$

in which is evident that a different derivative should be computed for every polarization.

With regard to the influence of an error on the knowledge of the complex dielectric constants, involved in the scattering matrix too, at the moment this is a work in progress.

Some considerations about the importance of the error in (4.13-15) are now in order. For the sake of simplicity, let us focus our attention on the particular case of φ=0, i.e. on (4.15). This allows us to not consider, for the moment, the influence of the angles and of the correlation length. More general results for $\varphi \neq 0$, obtained by means of simulation examples, are presented in the next Section. From (4.15) we see, for example, that a relative error of 10% on the knowledge of standard deviation leads to an error of 20% on the building height. It means that an error of a few centimeters on the standard deviation can lead to an error of some meters on the building height.

This expected result, confirmed by simulation examples, can be improved according to some considerations which implicitly told us when and where the deterministic method for building height extraction can be applied. We said that, in our method, the height of two buildings has to be known in order to radiometrically calibrate the SAR image [8]. This operation aims at making the measurements independent of the employed instrument and lies in determining two constants, one multiplicative, due to unknown signal amplification and attenuation, and the other additive, due to the background noise, also called 'offset error', see [8]. Now, let us suppose that the buildings used for calibration, and those whose height has to be retrieved, are all placed on soils with the same roughness parameters. For this instance, an imperfect knowledge of such parameters is not influent on the final result because the error they bear will be embedded in the multiplicative calibration constant. This consideration represents a guide line

in choosing a good set on the SAR image for which a deterministic extraction of building height can ensure accurate results.

Actually, errors due to the imperfect knowledge of different parameters are never isolated. But the influence of a simultaneous occurrence of errors is very difficult to be investigated by means of quantitative analysis of error propagation.

4.4.2 Empirical analysis

Now, our aim is comparing errors occurring on building height retrieval by deterministic approach on simulated SAR images with those expected by applying a quantitative analysis as explained in § 4.4.1. These first studies are interesting for a better understanding of future applicability of feature extraction method at real SAR images.

We considered again the canonical scene constituted by three buildings on rough terrain. Radar parameters adopted in simulations are typical of airborne sensors, with a carrier frequency of 1.282 GHz. Scene parameters, are the same of Table III except for the heights that are now, respectively, 30, 20 and 10 meters.

In simulation examples, we let φ vary from 20 to 40 degrees with steps of 5 degrees and observed changes in height extraction of central building when an error of ±10% on real value is considered for standard deviation σ. The errors Δh_T have been obtained by theoretic analysis by means of Eqs. (4.13-14) substituting h with the real value of the central building height (i.e. 20 m). These errors have been compared, in Table VI, with those deriving by simulation examples, Δh_S. The term Δh_S is the difference between the height that we would have retrieved for $\Delta\sigma$=0, which is already affected by calibration errors, and that one retrieved for $\Delta\sigma$=±0.019m.

Table VI

Theoretic error vs. simulation error.

φ [degrees]	Δh_T [m]	Δh_S[m], $\Delta\sigma$ =0.019 m	Δh_S[m], $\Delta\sigma$ =-0.019 m
20	±4.39	4.62	-4.20
25	±4.59	3.64	-3.31
30	±4.83	3.68	-3.36
35	±5.09	3.70	-3.38
40	±5.36	3.41	-3.12

Table VI needs some comments. Results deriving from theoretical analysis appear, in general, more severe than those measured on simulated SAR images. It can sound strange because the theoretical error on building height we compute by Eq. (4.13) is really due only to the error on deviation standard and is not affected by error in calibration or in the operation of extracting double reflection on the SAR image. Instead, these errors are intrinsically present in the procedure of building height extraction and surely affect the measure of Δh_S. Moreover, according to Table VI, increasing of the angle φ seems not to particularly affect simulation errors like theoretical ones.

For a better understanding of efficiency of the proposed approach, in Tables VII and VIII the comparison is made directly between the expected and the retrieved heights. Tables VII and VIII are relevant, respectively, to $\Delta\sigma$=+0.019m and $\Delta\sigma$=-0.019m. The errors committed respect to the real height value, called h_{TRUE}, are also indicated. Obviously, for both Tables VII and VIII, the third column agrees with the second one of Table VI. We note that, except for one case in Table VII, in general the retrieved height is better than the expected one. But, as we already said, more errors have been actually taken into account in the simulation examples. So, we are now wondering whether the presence of further errors on our knowledge of ground truth can indeed improve, and not worsen, the building height retrieval. The presence of multiple errors is at the moment under study by means of simulation examples as, for this case, theoretical analysis seems a way that can not be proposed.

Table VII

Comparison between expected and retrieved heights. Δσ=0.019m.

φ [degrees]	h_T [m]	$\Delta h_T=h_T-h_{TRUE}$ [m]	h_S [m]	$\Delta h=h_S-h_{TRUE}$ [m]
20	24.39	4.39	27.87	7.87
25	24.59	4.59	22.51	2.51
30	24.83	4.83	22.29	2.29
35	25.09	5.09	24.41	4.41
40	25.36	5.36	23.35	3.35

Table VIII

Comparison between expected and retrieved heights. Δσ=-0.019m.

φ [degrees]	h_T [m]	$\Delta h_T=h_T-h_{TRUE}$ [m]	h_S[m]	$\Delta h=h_S-h_{TRUE}$ [m]
20	15.61	-4.39	19.05	-0.95
25	15.41	-4.59	15.56	-4.44
30	15.17	-4.83	16.43	-3.57
35	14.91	-5.09	17.33	-2.67
40	14.64	-5.36	16.83	-3.17

Table IX

Height retrieval and relative error. Building orientation is extracted from the SAR image.

φ	h[m]	e[m]	$\varphi_1,\varphi_2,\varphi_3$	$\Delta\varphi_1,\Delta\varphi_2,\Delta\varphi_3$	h [m]	e[m]
15°	18.38	-1.62	19.5°; 21.8°; 17.6°	4.5°; 6.8°; 2.6°	19.93	-0.07
20°	23.25	3.25	26.6°; 24.0°; 19.5°	6.6°; 4.0°; -0.5°	22.32	2.32
25°	18.87	-1.13	27.4°; 29.8°; 26.6°	2.4°; 4.8°; 1.6°	20.66	0.66
30°	19.79	-0.21	29.8°; 29.8°; 34.7°	-0.2°; -0.2°; 4.7°	18.79	-1.21
35°	20.71	0.71	36.1°; 38.7°; 41.7°	1.1°; 3.7°; 6.7°	21.56	1.56
40°	19.95	-0.05	51.5°; 40.2°; 41.1°	11.5°; 0.2°; 1.1°	16.31	-3.69

In this framework, we also want to better detect the influence on the building height retrieval deriving from an imperfect knowledge of the angle φ.

Even if the calculation in Eq. (4.18) is not completely developed, it is possible to point out the direct proportionality between the building height and the error Δh, meaning the higher the building the bigger the error on height retrieval deriving from an error on the knowledge of φ.

At this point, transmitting and receiving polarization modes need to be set for completing the computation of the derivative in Eq. (4.18). Even if it showed to be intricate, for sake of completeness it has been done at least for HH polarization; but, the final expression is so complex to not encourage its use in evaluating the error on h resulting from an imperfect knowledge of φ.

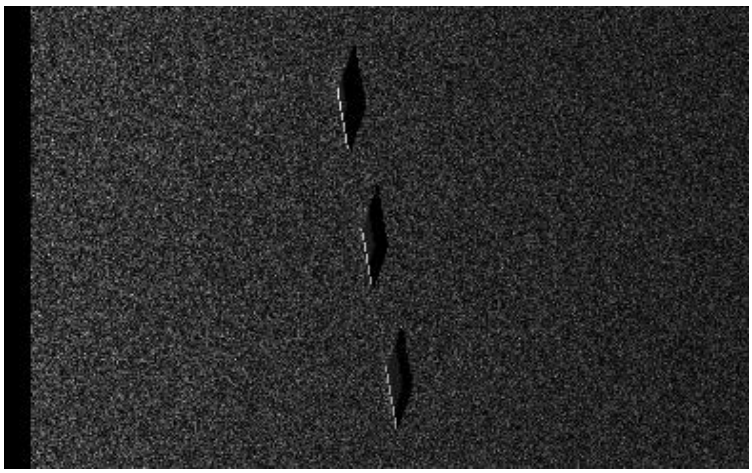

Figure 10 Simulated SAR image relative to an urban scene with buildings walls oriented at 35° respect to the radar flight trajectory.

For this reason, we preferred to carry on empirically the sensitiveness analysis, supported by simulation examples but aware that such a methodology if, on one side, is simpler than theoretic analysis, on the other it is not able to lead to very general conclusions.

The simulations have been set according the same radar and scene parameters of the previous example, except for the angle φ.

In Fig. 10, the simulated SAR image, relative to a scene in which φ=35° for all buildings, is shown.

In the simulation examples we let φ vary from 15° to 40° with a step of 5° (column 1 in Table IX) and we carry on the height retrieval in three different ways for.

The first time the central building height has been retrieved in absence of error on φ. The relative results are listed in column 2 of Table IX.

Secondly, we supposed unknown the angle φ and we tried to extract it from the simulated SAR images in azimuth and slant range coordinates according to the expressions:

$$\varphi = tg^{-1}\left[\frac{d_y}{d_x}\right], \tag{4.19}$$

$$d_y = \frac{d_r}{sen\vartheta} \tag{4.20}$$

where d_r and d_x represent the lengths of the segments marked in Fig. 11 and, in particolar, d_r is the projection of d_y in the azimuth/slant range coordinate plane.

The retrieved values of φ and the relevant heights are listed, respectively, in columns 3 and 5 of Table IX. Looking at these results we note that the angle φ is usually overestimated according a variable amount that is less than 7° in 95% of the events (column 4 in Table IX).

In fact, a statistic analysis shows a mean error of 3.4° and a standard deviation of 3.1° on φ estimate. Actually, as Eqs. (4.19-20) show, being this valuation strongly linked to the azimuth and slant range resolutions (respectively of 2.57 m and 4.84 m in the considered simulations) we can believe that it will certainly improve with the forthcoming launch of new high resolution SAR sensors.

These results lead to some considerations about the height retrieval.

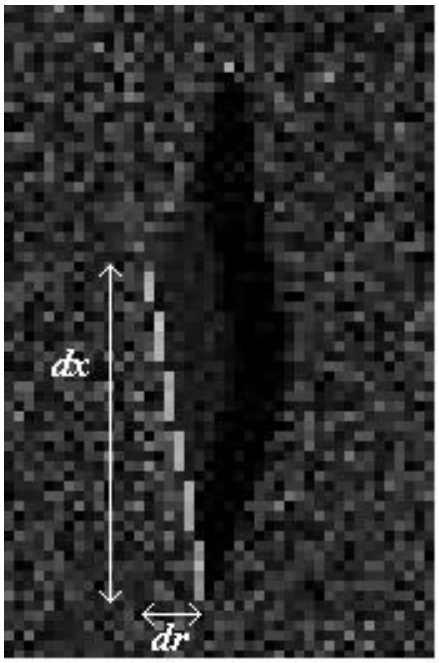

Figure 11 Zoom view of a building in Fig. 10.

The first one is that, in spite of the presence of errors in the knowledge of the three building walls orientations, it is still possible to extract the central building height with an error less than 2.5 m in the 80% of situations (column 7 in Table IX). Moreover, in the 50% of events, the retrieved h is even better than that extracted when φ is known (see columns 3 and 7).

But results in Table IX can not allow to well understand consequences on the height estimate because errors of different nature are taken into consideration at the same time.

In order to determine how the error on h depends upon the error on φ we must evaluate one error at a time. At this aim, we repeated the experiment supposing to evaluate only the angle φ of the central building with an error of 5°. Results on height retrieval and relative error are listed in Table X.

Table X shows that the errors on h and φ have the same sign. Even if this result can not be simply deduced by Eq. (4.18) it can be explained noting that, with φ increasing, the backscattering towards the radar decreases, so that a stronger contribution is related to a bigger height. Moreover, the error seems to be worsen for bigger orientation angles. A similar tendency could be noted also in results in Table IX. It is interesting to note that the error in Table X is always worsen than the one obtained when all buildings orientations are unknown.

These kinds of analysis, both theoretic and empirical, have been lead supposing some parameters unknown, like those ones describing the soil roughness or the building wall orientation, but the procedure is completely general and can be adopted, without further complications, also for the electromagnetic parameters involved.

Table X

Height retrieval and relative error. Central building orientation is known with 5° error.

φ	φ_1, φ_2, φ_3	h_{ephi} [m]	e [m]
15°	15°; 20°; 15°	20.67	0.67
20°	20°; 25°; 20°	27.25	7.25
25°	25°; 30°; 25°	22.23	2.23
30°	30°; 35°; 30°	23.54	3.54
35°	35°; 40°; 35°	24.55	4.55
40°	40°; 45°; 40°	23.20	3.20

4.5 Limits of applicability

In this Chapter the deterministic approach of feature extraction from a single SAR image has been presented. In order to discuss the reliability of the method it has been also applied to simulated SAR images for some extraction examples.

Now, the hypotheses that underlie this approach and the first retrieval results need some comments in order to identify the limits of applicability at a real SAR image.

We remind that, in all examples, we built canonical urban scenes in which all the present buildings had to be isolated in electromagnetic sense, i.e. their contributions to the (processed) SAR image did not overlap. It means that, for an application to real SAR images, we should mainly take into consideration "open spaces" where, effectively, the selected structures have free areas in front of them. This allows to the signal coming from the sensor to not be captured but to go back to the radar with an information that is quite well represented by the equations introduced in [1] and here inverted.

A particular extraction has been carried on in this Chapter and it is the building height retrieval from radiometric parameters measurable on SAR images.

But we want to stress again that this is only a possible example and that many other parameters (both geometric and electromagnetic) can be retrieved in theory, being the proposed extraction a model-based approach in which all the relationships among the parameters describing the scene are known and can be inverted, even if this operation is not always simple being many relationships not linear.

As often happens, sometimes the benefit of an approach turns also to be its limit. In fact, the knowledge of relative influence among parameters means that a high a-priori information of the scene under observation is needed for the extraction of only one parameter. Some unknowns can be retrieved by the SAR image itself but for many others we can only rely upon a previous knowledge hoping that it is still consistent with the ground truth.

When this knowledge is missing or not reliable, the feature extraction could be compromised.

To better understand these situations, a sensitiveness analysis has been carried on to study the eventual error propagation. In the particular feature extraction considered, for example, has been shown that an imperfect knowledge on roughness parameters can not influence the process of retrieval provided that the soils in front of the buildings are characterized by

the same roughness. This can be a guide line in choosing the building candidates in the real SAR image, as it will be in the next Chapter.

References

[1] G.Franceschetti, A.Iodice, D.Riccio, "A canonical problem in electromagnetic backscattering from buildings", *IEEE Trans. Geosc. Remote Sensing*, vol.40, pp.1787-1801, 2002.

[2] G.Franceschetti, A.Iodice, D.Riccio, G.Ruello "SAR raw signal simulation for urban structures", *IEEE Trans. Geosc. Remote Sensing*, vol.41, pp.1986-1995, 2003.

[3] G.Franceschetti, R.Guida, A.Iodice, D.Riccio, G.Ruello, "Deterministic Extraction of Building Parameters from High Resolution SAR Images", *Proceedings of the 3rd RSS/ISPRS joint Symposium on Remote Sensing and Data Fusion over Urban Areas,* Tempe (Arizona, USA), 2005.

[4] A.J.Bennett, D.Blacknell, "The Extraction of Building Dimensions from High Resolution SAR Imagery", *Proceedings of the International Radar Conference 2003*, pp.182-187, 2003.

[5] T.Pavlidis, *Structural pattern recognition*, Springer-Verlag, 1977.

[6] G.Franceschetti, R.Guida, A.Iodice, D.Riccio, G.Ruello, "Accuracy of Building Height Estimation from SAR images", *Proceedings of the International Geoscience and Remote Sensing Symposium*, Denver (Colorado, USA), 2006.

[7] Z.Xia, F.M.Henderson, "Understanding the Relationships Between Radar Response Patterns and the Bio- and Geophysical Parameters of Urban Areas", *IEEE Trans. Geosc. Remote Sensing*, vol.35, pp.93-101, 1997.

[8] Clair L. Wyatt, Radiometric Calibration: Theory and Methods, New York: Academic, 1978, pp.79-84.

Chapter 5

Applications to real HR SAR images

In the previous chapters, the deterministic approach for feature extraction from high resolution SAR images has been introduced, discussed and its feasibility has been analyzed on simulated SAR images relevant to canonical urban scenes.

Application to *real* SAR images is now in order.

Obviously, we are aware that this is only a first attempt and many other efforts should be done to assess definitively the conditions for the applicability of the proposed approach.

So, the aim of this Chapter is not telling a final world on the method efficiency but beginning to verify, in the *real* word, those limits, benefits and work conditions that have been just extensively argued.

The real SAR images shown in this thesis are a courtesy of the Technische Universität München (TUM) (Germany), currently involved with the University Federico II of Naples and University of Pavia in a research project for monitoring urban areas by SAR sensors (the Vigoni Programme). The above universities are also jointly involved in a project for the exploitation of TerraSAR-X data when they will become available.

The images have been acquired by airborne sensors but the missions parameters have been planned in order to achieve final resolutions in the order on 1 meter, as TerraSAR-X will grant. Also radiometric resolution is high being these ones 16-bit images (which means 65536 grey levels despite of 256 possible values of 8-bit simulated SAR images of Chapter 4).

They are relative of a central area in Munich (the area with the Alte Pinakothek) and a suburban area near the little village of Oberpfaffenhofen. Both the sites have been visited and studied more times in order to collect as more information as possible about the buildings in the scenes. Despite of this, some information is still missing but we tried to go around this problem exploiting the results of the previous analyses.

An example of geometric information retrieval is given in §5.1. The way we worked on the real image is explained and the results are discussed.

In §5.2 the foundations for electromagnetic parameter retrievals are laid and the interesting perspectives are remarked.

5.1 Building height retrieval in Oberpfaffenhofen area

In order to apply the deterministic approach for feature extraction we looked for an area satisfying the requirements previously highlighted: quite open spaces with buildings similar to big boxes represent the elected scenes.

In Figure 1 a scene with the above specifics is pictured. It is the airport area of the German Aerospace Center (DLR) located near Munich, more precisely close to the village of Oberpfaffenhofen. We can clearly distinguish the strip from which the airplanes leave for flight campaigns, some airplanes parked and many buildings characterized by quite simple shapes. To our intent the most interesting are represented by those ones which directly appear on the strip and which are labeled, in Figure 2, as the buildings n.386-373-324-390-338-310-316. To them we will refer in the following.

We know that the above buildings are not really parallelepipeds because mainly of the slope roofs but, actually, visiting the site, we realized the slope to be very low for some of them that have been consequently selected.

As regards the soil around the buildings, we can say without any doubt that they are placed on grounds with the same roughness and dielectric constants. In fact, in front of all them, we note an asphalt area followed by some grass. So, according to the considerations in Chapter 4, we know that an imperfect knowledge (both geometric and electromagnetic) on these materials will not affect our extraction as the contribution relative to this area will be absorbed in the calibration constant.

Application of the deterministic approach to a SAR image relevant to the scene in Figs.1-2 needs two key works: the first is the visit of the site to collect information on the ground truth that will be employed in the inversion procedure, the second is an accurate post-processing of the SAR image in order to measure those parameters from which the buildings heights will be retrieved. Both the steps are described in the following.

5.1.1 Visit of the site

The site in Fig.1 has been visited on 13 July 2006. The aim of the visit has been collecting information useful in the phase of building height retrieval from radiometric parameters.

Figure1 The DLR airport area in Oberpfaffenhofen (Germany). View from the top.

Figure 2 The DLR airport area in Oberpfaffenhofen (Germany). Lateral view (Courtesy DLR).

We remind that the extraction is planned to be carried on from the double reflection contribution to the radar cross section according the relationship in Eq.(4.4).

Then, it is logical to look at that expression to know which radar and scene parameters are involved and need, consequently, to be known or to be taken information on.

As far as concerns the SAR parameters we need knowledge essentially on the radar look angle θ, the working frequency f and the transmitting and receiving polarization modes, but they will be presented in the next paragraph together with the SAR image.

From the image itself we will recover the building orientation respect to the radar flight trajectory (the angle we called φ in the previous chapters) and the grey levels of the double reflection lines that are directly proportional to the radar cross section σ^o. This is also a task that will be made next.

As regards the scene, we require to know the buildings heights h, and the materials of the frontal walls.

We underline that knowing the materials does not imply knowing their dielectric constant ε_w as, unfortunately, the literature on the topic is still poor. In fact, the computation of this parameter depends strictly by many factors as the working frequency or the water content.

Empirical models for computing dielectric constants have been developed for some materials [1], above all for natural ones like grass, different kinds of soils, ice, lake water and so on. But for artificial materials (glass, plastic, concrete, asphalt etc..) these models are still insufficient and often inexistent.

Visiting the site, for each building we took general pictures of the entire structure and, closely, of the frontal wall to inspect the materials.

Being our intent to show the results of a first application of the retrieval approach proposed, we limit here to report the features and describe the structures only of two buildings, precisely the building n.310-338.

Actually, we know from the theory that we need of at least three buildings for a height extraction (two buildings stand for calibrators and the third is the one whose height is extracted).

But in this case, we will show that is possible to work with only two buildings as one, properly “decomposed”, will be sufficient for the calibration.

From Figs.3-4 some considerations can be derived about the selected buildings.

As far as concern the geometry, we note that, as anticipated, the slope of the roof is really low for both the buildings and that, consequently, the approximation of flat roof can be assumed without significantly affecting our procedure as can be shown in the following.

The front walls are constituted by big sliding doors. In both buildings, these doors are not aligned with the upper side of the building but they are indented. This difference respect to the geometrical model adopted in Chapter 4 does not represent a problem but it is necessary to take it into consideration to adequately apply our inversion.

(a)

(b)

(c)

Figure 3 Building n.310. Frontal view (a), a particular of the sliding doors (b), upper side of the wall (c).

(a)

(b)

(c)

Figure 4 Building n.338. Frontal view (a), a closest picture of the wall (b), a particular of the sliding doors (c).

Comparing different optical images, for the building n.310 the sliding doors and the highest extension of the upper side have been measured to be, respectively, 9.6 m and 3 m high.

For the building n.338, instead, the sliding doors and the highest extension of the upper side are, approximately and respectively, 5.5 m and 2.5 m high.

As regards the materials, the sliding doors are made of plastic windows and aluminium. In the building n.310, see Fig.3, they have, on both sides, a concrete tower and, on the top, a big plastic window. In the building n.338, instead, the upper side is in concrete and the sliding doors are separated with a material that seems to be concrete too but has been not clearly identified yet.

This information represents our knowledge of the ground truth. It will be used in the next paragraph for the inversion procedure.

5.1.2 Heights retrieval

After having analyzed the optical image of the area under study and collecting some information on ground truth, we can now move to inspect the relative SAR image.

It is shown in Figure 5. This type of image really represents a prototype of the products that will be available with the launch of new sensors. In fact, it is a high resolution SAR image (1.99m in range x 1.80m in azimuth) acquired on 20/04/2004 by an airborne SAR sensor during a flight campaign in the area of Oberpfaffenhofen.

It has been obtained with the radar working in X-band (9.6 GHz), a look angle of 55° and using vertical polarization for both transmitting and receiving modes.

Actually, the original SAR image is a 16-bit image which means 65536 grey levels but showing the image in its original format is not useful as the most of the contributions are in the low scale of the relative histogram. So, the 16-bit image would appear completely dark.

In order to see something in the image, we processed it with a byte scale operation in which we chose to represent the first 1000 grey levels of the original image with 256 levels. The image in Fig. 5 is the result of this elaboration.

Obviously, this has been done only to visualize the image because for the height retrieval, which is based on radiometric parameters, we exploited all the radiometric resolution working on the original image.

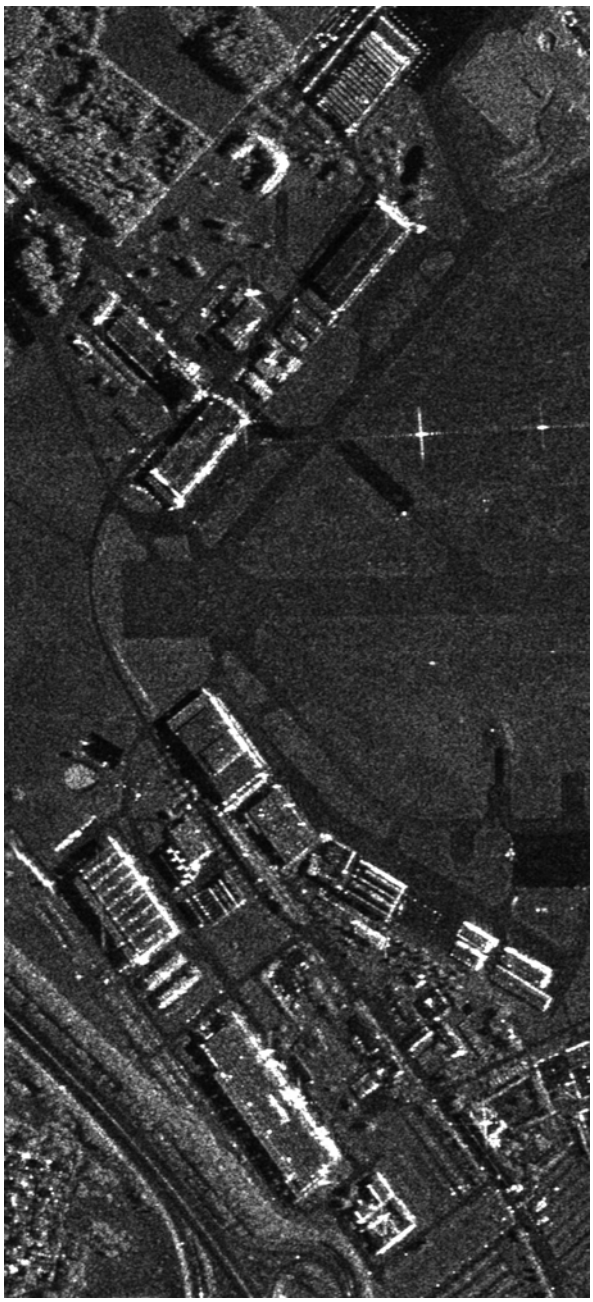

Figure 5 SAR image relative to the scene in Fig. 1 acquired on 20/04/2004. Image resolution: 1.99m (range) x 1.80m (azimuth). The radar trajectory is aligned with the right side of the picture.

The byte-scaled image has been used, in practice, only to correctly visualize the double reflection lines which have been, successively, localized and extracted from the original image.

As Fig. 5 shows, this artifact brings the double reflection contributions to saturation and to appear larger than they are. So, to avoid problems in selecting the right pixels, experiments with different byte scales have been carried on for a correct extraction.

The particulars visible on the SAR image, thanks to the very fine resolution, are really surprising. The main structures and the strips are all clearly evident but, looking better, we realized that it would have been possible to retrieve information that in previous SAR images we would have never seen.

An example is given by how the building n.310 appears in Fig.6.

Without any difficulty we can distinguish three double reflection lines. The shorter is caused by the little structure placed on the roof of the building that can be distinguished also in the optical image in Fig. 2. The division in the main façade in sliding doors and upper window are responsible, instead, for the two longer double reflection lines. In fact, as the doors are indented respect to the upper side, this geometry causes two close lines.

That is why we needed, in this particular case, of only one building for the calibration of the SAR image.

We measured the luminosity of these lines and we found for the inner one, relative to the big doors (9.6m high), a mean value of 2568 while, for the outer one relative to the upper side (3m high), a mean grey level of 786 has been measured.

Computing the ratio between the heights above and the ratio between the grey values in the corresponding double reflections, we find very similar values (respectively 3.27 and 3.20) which is a first good result on the proportionality we expected to have.

In the future, the retrieval of the height of the upper structure will be attempted when some information on the roughness roof will be available.

In the SAR image, the building n.338, having a structure very similar to that of building n.310, should also contributes with two lines but this time it is not so evident. The clearest line contributes with a mean value of 629. The inversion procedure, in this case, retrieves a height of 2.6m. This value seems to correspond to the upper side of the front wall which measures about 2.5m. The measure of the doors height has not yet carried on.

These results are not yet sufficient to definitively assess the effectiveness of the inversion procedure but the extraction of all the double reflection lines in the SAR image is currently a work in progress to carry on further verifications.

Figure 6 Enlarged view of the bottom side of Figure 5.

5.2 The site of the Alte Pinakothek in Munich: first steps in electromagnetic parameters retrieval

Geometric information retrieval from a single real high resolution SAR image of urban areas has been introduced in the previous paragraph.

Now, we would like to inspect whether a similar inversion can be applied in future for retrieving information about the electromagnetic

parameters describing the scene (or, equivalently, about the materials characterizing the structures in the scene).

To this aim, we are currently carrying on an interesting study on the area of Schwabing, in the heart of Munich (Germany), more precisely on the building of the Alte Pinakothek. This is the structure in the red frame in Fig.7.

The SAR image relevant to the scene in Fig.7 is reported in Fig. 8. it has been already byte scaled.

In this case we worked differently respect to the SAR image in §5.2. in fact, there we first collected information on the ground truth and then applied the inversion procedure.

Here, instead, we first analyzed the SAR image observing some interesting effects and then we tried to guess what we expected to find visiting the site. Finally, we checked our hypothesis.

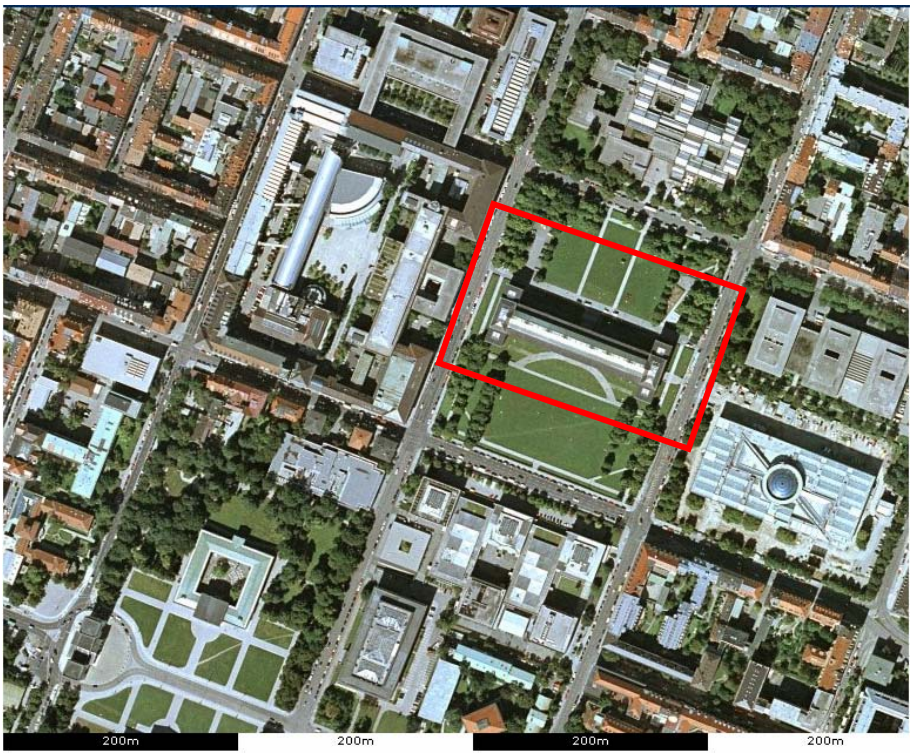

Figure 7 Optical image of Schwabing in the centre of Munich (Germany) with the Alte Pinkothek

The only thing we knew about the building of the Alte Pinakothek was that the structure is perfectly symmetric in shape.

Now, in the SAR image of Fig. 8, the sensor flies along the bottom side of the image, as can be clearly deduced from the shadow areas.

The open space in front of the picture-gallery allows us to consider this building quite isolated in the meaning explained in Chapter 4.

Looking at the image, we note that the double reflection line appears not continuous in its intensity. This seemed to be strange considering the symmetry of the building.

In other cases we would have referred the different intensities to different heights. But being this impossible, for the hypothesis of geometrical symmetry, only an alternative remained: assuming the presence of an *electromagnetic* dissymmetry in the front wall.

This supposition was the only acceptable considering again the theory presented in Chapter 4 and, in particular, Eq.(4.4) here reported for sake of simplicity:

$$h = \left|\sigma^{\circ}\right| \frac{8\pi^2 \cos^2 \vartheta \cdot \sigma^2\left(2/L^2\right) \cdot \exp\left[\dfrac{\tan^2 \vartheta \sin^2 \varphi}{2\sigma^2\left(2/L^2\right)}\right]}{\left|S_{pq}\right|^2 l \tan \vartheta \cos \varphi \left(1+\tan^2 \vartheta \sin^2 \varphi\right)}$$

Figure 8 HR SAR image relative to the scene in Fig. 7.

According to the expression above if the geometrical parameters are the same for the two sides (having the same height h, the same orientation φ respect to the radar flight trajectory), if these sides are placed on a ground with the same roughness (described by σ and L) and the same electromagnetic behavior (ε_s in S_{pq}), then only the presence of different materials in the front wall (ε_w in S_{pq}) can explain the discontinuity in the double reflection line.

Figure 9 demonstrates that this hypothesis is true.

It represents a particular of the front wall, precisely the right side. The main door corresponds to the centre of the wall. We note the presence of different materials just where it was expected. In fact, built in 1836, the Alte Pinakothek was severely bombed during the second world war [2]. But the architect Hans Döllgast, engaged in the ‘50s for the restoration of the gallery, did not reconstruct the building from the beginning. He used together some old bricks coming from the ruins and new ones and backed the wall with steel pipes because he thought that the wounds of a war have to remain visible to help people to keep the memory alive.

Figure 9 A picture of the south wall of the Alte Pinakothek in Munich (Germany)

Now, if we look closely Fig. 8, we can number seven sparkling points. Looking again at Fig. 9, we number seven steel pipes. So, it seems that information on electromagnetic parameters can be really retrieved from high resolution SAR image.

In order to have some confirmation of the theory above, a simple scene similar to the real one has been simulated too, [3].

A geometrical structure similar to that of the Pinakothek has been assumed for the central building but different materials have been assigned to the two sides of the same wall, precisely bricks at the upper side and steel at the lower side.

The resulting simulation is shown in Figure 10. The brightest double reflection where the steel side is present is consistent with the analysis performed on real SAR images.

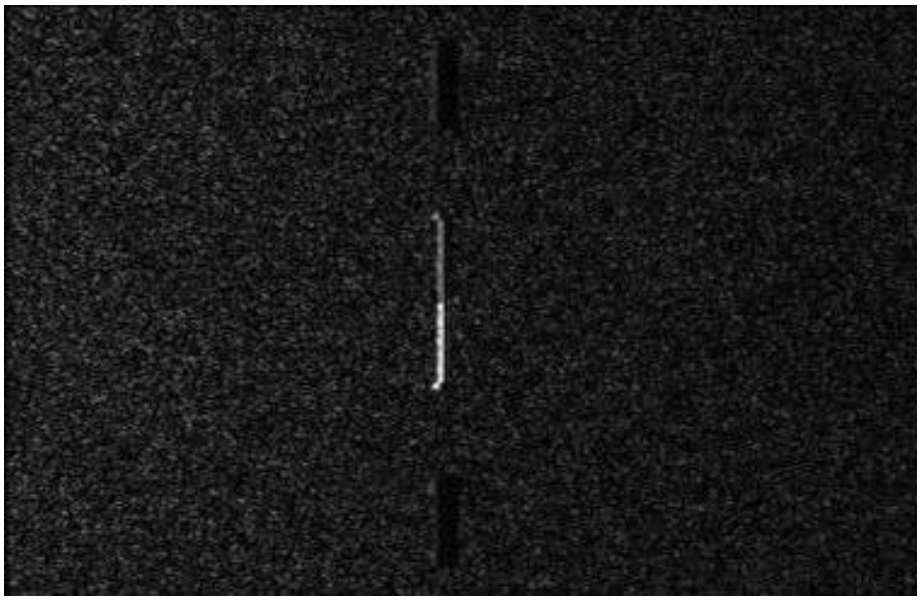

Figure 10 A simulated SAR image relevant to a scene with a building having the same geometry of the Pinakothek and different materials (bricks and steel) in the two sides of the same front wall.

5.3 Future perspectives

In this Chapter we tried to inspect the application of the deterministic approach for feature extraction to real SAR images of urban areas.

The capability of this method of studying new aspects and details of the SAR urban images is due mainly to the high resolution on one hand and to a model-based inversion approach on the other.

Some examples have been carried out but the results allow us to generalize and discuss what we could expect by future research in this topic.

As regards the geometric parameters retrieval, we are progressing well on building dimensions also because the effectiveness of our method can be often checked comparing our results with those deriving from different approaches. But our analysis must be still refined, above all in the sensibility analysis, for a better understanding of the influence of an imperfect knowledge of the ground truth (shown to be the weak side of our inversion procedure).

In theory, soil roughness could be retrieved too (see Table I in Chapter 4) and information could be extracted exploiting as many contributions as possible on the SAR image (for example, the single scattering from the ground as well as the double reflection).

As far as concerns the electromagnetic parameters, the interest on the possibility of retrieving this kind of information is high for the reasons we explained in Chapter 3.

Here, we limited to some considerations lead by the model-based approach. In future we would verify them in practice, trying to retrieve (this time by a couple of SAR images) the real and imaginary parts of the complex dielectric constants.

This represents a really hard task but also an interesting challenge that could completely change our way of looking at SAR images.

References

[1] F.T.Ulaby, R.K.Moore, A.K.Fung, *Microwave Remote Sensing*, vol.III, Artech House, 1986.

[2] www.altepinakothek.de

[3] G.Franceschetti, R.Guida, A.Iodice, D.Riccio, G.Ruello, U.Stilla, "Simulation Tools for Interpretation of High Resolution SAR Images of Urban Areas", *Proceedings of the 4th RSS/ISPRS joint Symposium on Remote Sensing and Data Fusion over Urban Areas,* Paris (France), 2007.

Summary and conclusions

In this thesis the interesting topic of urban areas monitoring with high resolution SAR sensors has been discussed.

This work has been shown to originally contribute to the theme at issue, as ranges from the development of direct models for raw signals simulation to the proposal of new inversion methods for feature extraction from SAR images of urban areas.

Particularly, an efficient SAR raw signal simulator has been developed for the hybrid stripmap/spotlight acquisition mode, thus producing an important tool for supporting the design and realization of upcoming sensors working in this geometry as well as for testing processing algorithms when raw data are not yet available.

To this aim, a new transfer function has been defined and evaluated, via asymptotic expansion, for the hybrid case. After having shown the impossibility of working in the 2D Fourier domain, a monodimensional Fourier approach (for the range coordinate) followed by an integration in the time domain (for the azimuth coordinate) has been proposed when some approximations, usually verified in the real cases, are assumed.

The simulation scheme proposed appears much more efficient than a time domain approach and consequently allows to consider also extended scenes. With many simulation examples, relative to canonical scenes, the validity of the algorithm proposed has been tested.

On the topic of feature extraction from SAR urban images, a new deterministic approach has been proposed. It is based on geometrical models of urban areas and on a scattering model for computing, in closed form, the signal backscattered towards the radar. The relationships between the set of parameters (both geometrical and electromagnetic) to be retrieved and the set of parameters measurable on the SAR images have been highlighted and this knowledge has been exploited for the feature extraction.

The most interesting relationships have been inverted for the building geometrical parameters extraction, developing an independent equations system whose solution can lead to multiple determinations of the same parameter.

The effectiveness of the method proposed has been verified applying it to simulated SAR images of different built up areas (letting vary both the radar parameters and the scene features) and, for the first time in literature, the building height has been retrieved from radiometric parameters measurable on the SAR image. These results have been also compared with those deriving by different approaches already existing in literature.

Moreover, a sensitiveness analysis has been developed to evaluate the limits of applicability of the deterministic approach to real SAR images. In particular, as regards the building height extraction, the effects deriving on this evaluation from an imperfect knowledge of other parameters describing the scene have been inspected through a study of error propagation.

First results of the inversion procedure applied to real SAR images have been discussed. Retrieval of both geometric and electromagnetic parameters seems to be promising but the phase of testing is still now a work in progress and some issues need to be further explored in future work.